Light Water Reactor Sustainability Program

Online Monitoring of Induction Motors

Timothy R. McJunkin, Vivek Agarwal, Nancy J. Lybeck

January 2016

U.S. Department of Energy

Office of Nuclear Energy

Online Monitoring of Induction Motors

Timothy R. McJunkin, Vivek Agarwal, Nancy J. Lybeck

January 2016

**Idaho National Laboratory
Idaho Falls, Idaho 83415**

http://www.inl.gov

(This page intentionally left blank)

ABSTRACT

The online monitoring of active components in nuclear power plants project, under the Advanced Instrumentation, Information, and Control Technologies Pathway of the Light Water Reactor Sustainability Program, researched diagnostic and prognostic models for alternating current induction motors. Idaho National Laboratory (INL) worked with the Electric Power Research Institute (EPRI) to augment and revise the fault signatures previously implemented in the Asset Fault Signature Database of EPRI's Fleet-Wide Prognostic and Health Management (FW-PHM) Suite software. The revised set of induction motor fault signatures is presented in this report. Subject area experts from INL's Advanced Test Reactor were used to validate induction motor fault signatures based on vibration measurements.

To enhance the understanding of bearing-related faults in induction motors, an experimental study was performed on two 40-horsepower motors at Idaho State University's Energy Systems Technology and Education Center. Essential lessons were learned during the experimental procedure and are summarized in this report. Some of the initial findings from the experimental procedure were presented at the *2015 Joint Summer Utility Working Group* and *EPRI Strategy Group on Productivity Meeting* in Idaho Falls, Idaho.

(This page intentionally left blank)

SUMMARY

As nuclear power plants (NPPs) continue to age and their components degrade, it is important to understand their condition and be proactive in maintenance and replacement to improve plant reliability and productivity, and to reduce operational cost. The current maintenance practices at NPPs result in high maintenance costs and increased likelihood of human error. Additionally, the inability to identify developing faults can lead to either unexpected component failure and/or forced outage. Implementation of advanced predictive online monitoring (OLM) would minimize these concerns and enhance plant safety, reliability, and productivity by enabling plant maintenance engineers to diagnose incipient faults and estimate the remaining useful life (RUL) of assets.

The U.S. Department of Energy's Office of Nuclear Energy funds the Light Water Reactor Sustainability (LWRS) Program to develop the scientific basis for extending the operation of commercial light water reactors beyond the current 60-year license period. The program is operated in collaboration with the Electric Power Research Institute's (EPRI's) research and development (R&D) efforts in the Long-Term Operations (LTO) Program. The LTO Program is managed as a separate technical program operating in the Plant Technology Department of the EPRI Nuclear Power Sector with the guidance of an industry advisory integration committee. Both the LWRS and LTO programs work closely with nuclear utilities to conduct R&D in technologies that can be used to ensure long-term reliability, productivity, safety, and security of aging light water reactors.

Under the Advanced Instrumentation, Information, and Control Technologies Pathway of the LWRS Program, the OLM of active components project at Idaho National Laboratory (INL) focused on research, development, and implementation of diagnostic and prognostics models for induction motors, which are the workhorse for the mechanical pumps used in cooling systems of nuclear reactors. EPRI is leading the effort to achieve the project objective in collaboration with INL, using EPRI's Fleet-Wide Prognostic and Health Management (FW-PHM) Suite software (Version 1.2.0) for predictive OLM of active assets in the nuclear industry. The FW-PHM Suite software is an integrated suite of web-based diagnostic and prognostic tools and databases that allows maintenance staff to perform diagnosis and prognosis at different hierarchical levels, from the component level to the plant level, across a fleet of power units.

During Fiscal Year 2015, INL's research activities were focused on developing diagnostic models for induction motors in NPPs. Modern induction motors are very robust and reliable machines, but are susceptible to faults associated with the electro-mechanical components common to electric spinning machines. Specific faults are related to bearing wear and damage, rotor bar damage, air gap eccentricities and misalignment of coupled mechanical systems (e.g., pumps). As with other electrical equipment, deterioration of winding insulation is also possible, but it was not studied during this project. Instrumentation of induction motors may include temperature, vibration, and stator current. The vibration and stator current can be analyzed through various statistics and by harmonic analysis in the frequency domain. Signatures for degradation in induction motors have been well studied; however, the practical aspect of instrumenting and analyzing the sensor data for prognostics purpose has challenges in practice. This report highlights some of those challenges.

INL performed the following research activities:

- Reviewed literature of induction motor faults and monitoring techniques used to diagnose developing faults

- Explored the practical application of diagnostics through discussions with an INL subject matter expert responsible for determining faults on rotating machinery.

- Analyzed data from accelerated aging experiments in an attempt to determine viable RUL

- Instrumented an experimental platform, through a partnership with Idaho State University's Energy Systems Technology and Education Center, to develop fault signatures associated with bearing degradation

- Presented initial experimental finding at the Joint Summer Utility Working Group and EPRI Strategy Group on Productivity Meeting Idaho Falls, Idaho.

This project ends in March 2016; thus, no future research activities are planned.

ACKNOWLEDGMENTS

(This page intentionally left blank)

CONTENTS

FIGURES

TABLES

(This page intentionally left blank)

ACRONYMS

AC	alternating current
AFS	Asset Fault Signature
ATR	Advanced Test Reactor
CT	current transformer
DAQ	Data Acquisition
EPRI	Electric Power Research Institute
ESTEC	Energy Systems Technology and Education Center
FFT	Fast Fourier Transform
FW-PHM	Fleet-Wide Prognostic and Health Management
FY	fiscal year
IEEE	Institute of Electrical and Electronics Engineer
INL	Idaho National Laboratory
ISU	Idaho State University
LTO	Long-Term Operations (Program)
LWRS	Light Water Reactor Sustainability (Program)
MCSA	motor current signature analysis
NI	National Instruments
NPP	nuclear power plant
OLM	online monitoring
PLC	programmable logic controller
PSD	power spectral density
R&D	research and development
RMS	root mean square
RUL	remaining useful life
SME	subject matter expert
STFT	Short-time Fourier transforms
UTK	The University of Tennessee, Knoxville

(This page intentionally left blank)

1. INTRODUCTION

More than two-thirds of the existing commercial nuclear power plants (NPPs) in the United States have received license extensions to 60 years from the original 40-year license. As the fleet of NPPs continues to age, it is important to understand the condition of their aging components and be proactive in maintenance and replacement. The current practice of periodic and condition-based maintenance at NPPs could result in high repairs costs, primarily due to unexpected component failure and forced outage. Implementation of advanced predictive online monitoring (OLM) would enable plant maintenance engineers to diagnose incipient faults and estimate the remaining useful life (RUL) of their assets. Knowledge of asset health gained from predictive OLM would help in optimizing maintenance activities, ultimately leading to maintenance cost reduction.

The U.S. Department of Energy's Office of Nuclear Energy funds the Light Water Reactor Sustainability (LWRS) Program to develop the scientific basis for extending the operation of commercial light water reactors beyond the current 60-year license period. The program is operated in collaboration with the Electric Power Research Institute's (EPRI's) research and development (R&D) efforts in the Long-Term Operations (LTO) Program. The LTO Program is a separate technical program in the Plant Technology Department of the EPRI Nuclear Power Sector, which is guided by an industry advisory integration committee. Both the LWRS and LTO programs work closely with nuclear utilities to conduct R&D in technologies that can be used to ensure long-term reliability, productivity, safety, and security of aging light water reactors.

Implementation of predictive OLM of essential assets in the existing fleet of NPPs is supportive of the long-term objective of both the LWRS and LTO programs. Predictive (also known as proactive) maintenance requires predicting the future operating state of an asset based on the current state and historic operating conditions. For example, the consequence of running a transformer for an extended period with a high oil temperature is an unacceptable loss of dielectric strength of the insulating oil. Accurate estimation of a transformer's RUL accounting for high-temperature operating conditions would help maintenance staff take appropriate actions to prevent costly unplanned outage. Taking the lead in predictive OLM research, EPRI has developed the Fleet-Wide Prognostic and Health Management (FW-PHM) Suite software (currently at Version 1.2.0) for predictive OLM of assets in the power industry. The FW-PHM Suite software is an integrated suite of web-based diagnostic and prognostic tools and databases that enables maintenance staff to perform diagnosis and prognosis at different hierarchical levels, from the component level to the plant level, across a fleet of power units.

For fiscal year (FY) 2015, the project focused on induction motors—the primary drivers of rotational mechanical systems such as cooling pumps in the nuclear energy systems. Though very robust electro-mechanical machines, faults eventually occur due to degradation and maintenance issues. The faults and fault signatures, as well as potential remaining useful life quantifications, were studied in existing literature, through discussions with practitioners, and through experiments with representative motors.

During FY 2015 and early FY 2016, Idaho National Laboratory (INL) performed research to identify fault categories of induction motors, including a content development exercise to implement/update technical examinations, fault features, and fault signatures in the FW-PHM Database for induction motors used in NPPs. The fault features and fault signatures were developed based on data collected from experimental studies conducted at The University of Tennessee, Knoxville, the Advanced Test Reactor at INL, and Idaho State University. The data collected were associated with bearing-related failures. Other fault features and fault signature implemented/updated in the FW-PHM Database for induction motors were based on review of peer-reviewed journal and conference articles associated with faults and failures of induction motors. The experimental study at Idaho State University's College of Technology was performed on two identical 40-HP induction motors. Both the motors were fitted with identical sensors, including thermocouples, current transformers, and accelerometers to collect data. A National Instruments (NI) X Series Data Acquisition system was used to collect data in real-time. The data collected were

processed and monitored to detect any signs of degradation (anomalies) in the motor performance. For the purpose of this research, a loss of bearing lubrication fault was introduced in one of the induction motors, while the second motor was operated in a healthy state. The bearing lubrication was flushed, and the motor was operated for extended period of time with the expectation that the lack of lubrication would degrade the bearing. Temperature, vibration, and motor current data were continuously recorded, processed, and analyzed to detect any precursor(s) associated with loss of bearing lubrication. The details are discussed later in the report.

The project progress and status of research activities for FY 2015 are presented in this report. A brief introduction to the FW-PHM Suite is presented in Section 2. Section 3 summarizes induction motor instrumentation and the fault signature for inductions. The validation of fault signatures based on experimental data sets is presented in Section 4. The experimental data sets used to validate induction motor fault signatures were obtained from a laboratory scale experiment on induction motors. Finally, the research progress is summarized in Section 5.

2. FLEET-WIDE PROGNOSTIC AND HEALTH MANAGEMENT SUITE SOFTWARE

The FW-PHM Suite software is an integrated suite of web-based diagnostic and prognostic tools and databases, developed for EPRI by Expert Microsystems, specifically designed for use in the commercial power industry (for both nuclear and fossil fuel generating plants). The FW-PHM Suite serves as an integrated health management framework, as shown in Figure 1, managing the functionality needed for a complete implementation of diagnostics and prognostics (Lybeck et al. 2011). The FW-PHM Suite consists of four main modules: the Diagnostic Advisor, the Asset Fault Signature (AFS) Database, the RUL Advisor, and the RUL Database. The FW-PHM Suite has the capability to perform diagnosis and prognosis at different hierarchical levels, from the component level to the plant level, across a fleet of power units.
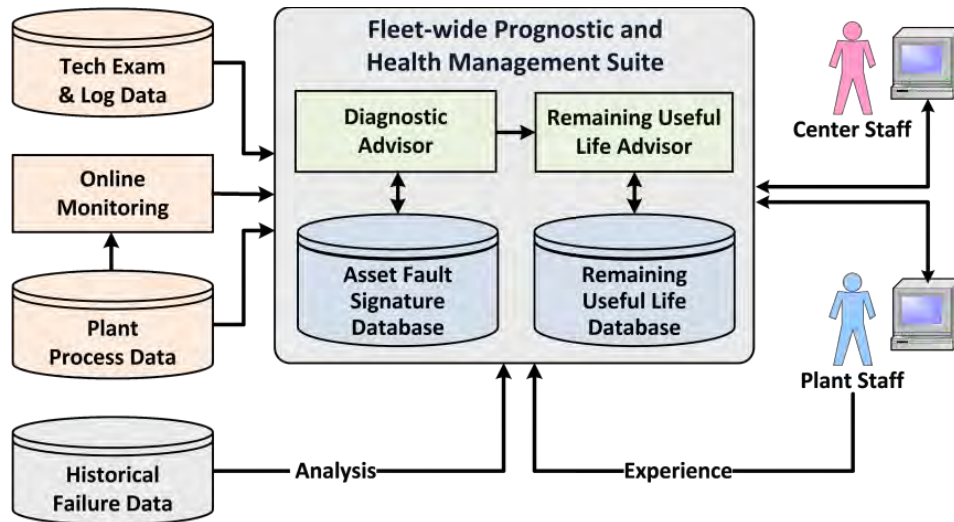
Figure 1. Data flow in the EPRI FW-PHM Suite (EPRI 2011b).

2.1 Asset Fault Signature Database

The AFS Database organizes fault signatures collected from the many EPRI member utilities. At the most basic level, fault signatures are comprised of an asset type, a fault type, and a set of one or more fault features (symptoms) that are indicative of the specified fault. Each installation of the software has two separate database schemas: the master database maintained and distributed by EPRI, and a local database containing data developed at the plants or fleet monitoring center. Locally developed

2

information can be exported and sent to EPRI for evaluation and possible inclusion in the master database that is shared amongst EPRI members. The AFS Database is populated via a content development exercise described in Agarwal et al., 2013 report.

2.2   Diagnostic Advisor

The Diagnostic Advisor identifies possible faults by comparing asset fault signatures with operating data. The Diagnostic Advisor is expected to be used on a daily or other periodic basis by technicians who are monitoring the health of a specific asset in the plant. Using either online data sources or information entered manually, the Diagnostic Advisor presents the likely faults (if any) and, when appropriate, recommends additional tests that might be used to discriminate amongst possible faults. The Diagnostic Advisor is expected to streamline the diagnosis process by helping the technician focus efforts on the most likely faults and possible causes based on the operating behavior of the system.

2.3   Remaining Useful Life Database

The RUL Database organizes asset RUL signatures (i.e., models) collected from across the industry. At the most basic level, a RUL signature is comprised of an asset type, a model type, and model calibration parameters. The model type definition includes definition of the input variables needed to run the model. Subject matter experts from the power industry, EPRI, and EPRI's partners/subcontractors will most likely develop RUL signatures. Figure 2 shows the modules available in the FW-PHM Suite software.

Figure 2. FW-PHM Suite main page.

2.4   Remaining Useful Life Advisor

The RUL Advisor calculates RUL for an asset based on the model type, model parameters, input process parameters, and diagnostic information (from the Diagnostic Advisor). The engineering staff and plant management who plan long-term corrective or replacement actions would use the RUL Advisor.

The FW-PHM Suite uses fault signatures as a structured representation of the information that an expert would use to first detect and then verify the occurrence of a specific type of fault (EPRI 2012). A fault describes a particular mode of degradation that can be detected by analysis of plant information before the asset fails to meet a service requirement. Implied is an assumption that the fault is detectable by analysis of plant information and that the analysis can be performed in time to prevent or otherwise remedy the fault condition before it becomes a failure condition.

Diagnostic fault signatures are developed for application to a specific type of asset and are therefore organized with reference to that type of asset. However, it is desirable to specify fault signatures as broadly as possible to be used in the entire industry. Many of the fault signatures defined in this research can be applied to comparable assets used in similar service environments.

3. INDUCTION MOTOR INSTRUMENTATION AND FAULT SIGNATURES BACKGROUND

Due to its simplicity and ruggedness, the induction motor is the most commonly used type of electric motor. Induction motors range in size from the fractional-horsepower, single phase motors found in household applications to the polyphase motors rated at thousands of horsepower used in industrial applications. As depicted in Figure 3 induction motors consist of a set of windings, known as the stator, that connect to an alternating current (AC) drive. A time varying magnetic field is generated by the current flow through the motor windings. Windings encompassing the three phases of the typical AC distribution are arranged to provide a circular rotation of the magnetic field as the cycles of the AC current progress. The stator is typically stationary. The rotor attaches to the shaft of the motor the exports mechanical power to the attached machinery. Bearings support the rotor and allow it to spin with a low amount of frictional drag. The rotor is comprised of a core of conductors that connect to the outside shorting ring through rotor bars that conduct induced current to a common point. The rotor core carries induced voltage due to the lag or slip in rotation of the rotor with respect to the stator poles, which in turn provides the motor torque as that current interacts with the magnetic field of the stator. Failures may be more prevalent in the moving parts that support the rotation of the motor due to wear, improper assembly or maintenance, or other damage.

3.1 Faults, Technical Exam and Fault Signatures for Induction Motors

There have been many investigations on condition monitoring and fault diagnostics in electric machines, especially squirrel-cage induction motors. This is because failure of such motors can lead to significant undesirable repercussions such as production downtime, financial loss, and possible personal injury. Considerable interest in machine fault diagnostics and prognostics received from the nuclear industry prompted investigation into online monitoring of induction motors.

3.1.1 Classification of Faults

Induction motors are subjected to various stresses such as thermal, mechanical, electrical, and environmental, which impact motor health and can lead to faults. Yeh et al. (2008) broadly classified various types of faults observed in induction motors, as indicated in Figure 4. The probability of occurrence of these faults is given in Table 1. For this research, the focus was on development of diagnostic and prognostic models for mechanical faults (i.e., air-gap eccentricity faults and bearing-related faults).

Bearing faults may be reflected in defects of outer race, inner race, ball, or track. Some of the main contributors to bearing faults are dust and corrosion. Induction motors are often operated in harsh conditions, resulting in exposure of the bearings to foreign materials, water, and humidity; contamination
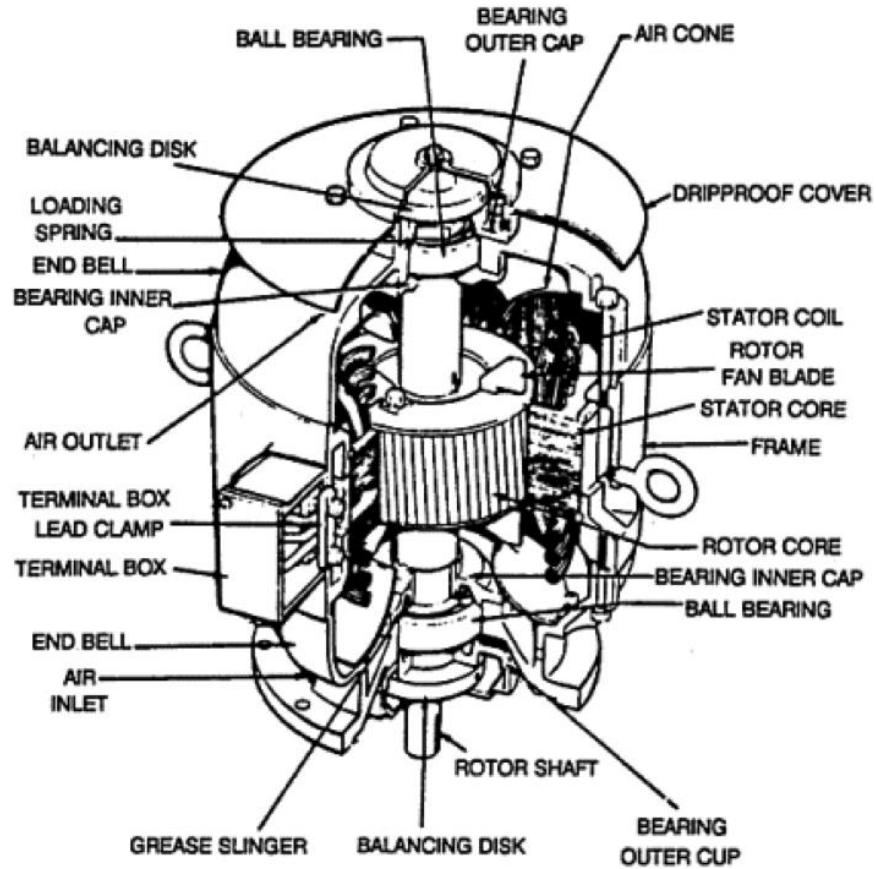
Figure 3. Different elements of induction motor
[http://www.pacontrol.com/image/three_phase_induction_motor.gif].

and corrosion are common in industrial settings. Dirt and other foreign matters that are commonly present often contaminate the bearing lubrication. The abrasive nature of these minute particles, whose hardness can vary from relatively soft to diamond-like, causes pitting and sanding that lead to measurable wear of the balls and raceways. Bearing corrosion is produced by the presence of water, acids, and deteriorated lubrication. Also, improper lubrication (including both under- and over-lubrication) results in bearing faults. In either case, the rolling elements are unable to rotate on the designed oil film, causing increased temperatures. This excessive heating causes the grease to break down, which reduces its ability to lubricate the bearing elements and accelerates the failure process.

Table 1. Percentage of failures by major motor components.

Major Component	IEEE-IAS (IEEE Committee Report 1985) % of Failures	EPRI (Albrecht et al. 1986) % of Failures
Bearing Related	44	41
Winding Related	26	36
Rotor Related	8	9
Others	22	14
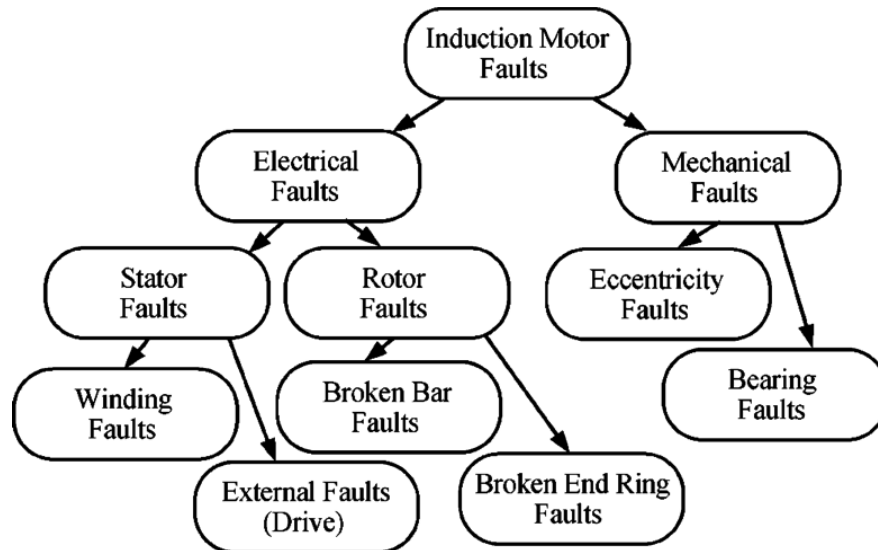
Figure 4. Induction motor fault classifications (Yeh et al. 2008).

Bearing problems are also caused by improperly forcing the bearing onto the shaft or into the housing. This produces physical damage in the form of brinelling or false brinelling of the raceways, which leads to premature failure. Misalignment of the bearing, which occurs in four ways, as depicted in Figure 5, is a common result of defective bearing installation. Ultimately, lubrication fatigue and mechanical wear lead to bearing failure.
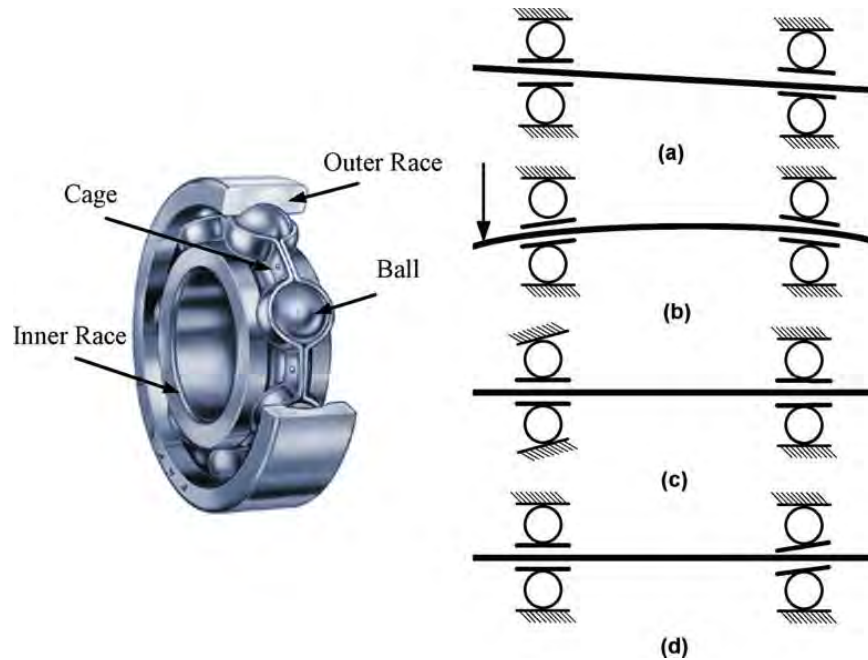
Figure 5. (a) Misalignment (out-of-line), (b) shaft deflection, (c) cocked or tilted outer race, and (d) cocked or tilted inner race (Onel and Benbouzid 2008).

Air-Gap Eccentricity: The air-gap of the motor is the space between the stator insulation and the rotor. The motors are designed such that the stator and the rotor cage are concentric cylinders, creating a consistent air gap. The consistency leads to uniform induction currents in the rotor bars and a uniform magnetic field with respect to the rotational position of the rotor. Eccentricity is a mechanical fault that

may include eccentricity in the rotor outer diameter or the stator inner diameter, differing axis for the rotor center of rotation and the stator, and/or misalignment of the rotor shaft with the rotor cage. Airgap eccentricity takes two basic forms: static and dynamic. Static eccentricity is characterized by a displacement of the axis of rotation where the position of the minimal air gap length is fixed in space. It can be caused by stator ovality or by incorrect positioning of the rotor or stator at the commissioning stage. Since the rotor is not centered within the stator bore, the field distribution in the air gap is no longer symmetrical. The non-uniform air gap gives rise to a radial force of electromagnetic origin, called unbalanced magnetic pull, which acts in the direction of minimum air gap. A bent shaft, mechanical resonances, bearing wear or misalignment, or even static eccentricity may cause this kind of eccentricity. Therefore, the non-uniform air gap of a certain spatial position is sinusoidally modulated and also results in an asymmetric magnetic field. This, accordingly, gives rise to a revolving unbalanced magnetic pull (Nandi, Toliyat, and Li, 2005).

Airgap eccentricity in induction machines causes characteristic harmonic components in electrical, electromagnetic, and mechanical quantities. Therefore, either mechanical quantities such as vibration, torque oscillations, or electrical quantities such as current or instantaneous power can be analyzed to detect eccentricity conditions (Kral, Habetler, and Harley 2004).

3.1.2   Technical Examinations

Given the fault classification in Figure 4, various monitoring methods or technical examinations (with respect to the FW-PHM) are used. These include:

- *Vibration.* Healthy induction motors produce only low-level vibration signals under normal operating conditions. When a fault in the internal parts of an induction motor occurs, large variations in vibration signals are generated. Monitoring vibration signals is considered to one of the most effective technical examinations for bearing faults detection. This can be achieved by attaching transducers to the bearings to measure vibration signals in all three directions. Monitoring vibration signals also allows detection of faults like unbalance mass, misalignment of rotors, as well as gear mesh problems of induction motors (Kral et al. 2003).

- *Electromagnetic field.* When an induction motor operates under normal conditions, sinusoidal variations in the air gap flux occur. However, asymmetric rotors or stators can lead to changes in signal variations. For condition monitoring of stators, a search coil (attached to the motor shaft) can be used to measure the distortion pertaining to the flux density of the air gap (Cameron, Thomson, and Dow 1986). For condition monitoring of rotors, an internal or external search coil can be used (Elkasabgy, Eastham, and Dawson 1992). It is preferred to detect signal variations by using an external stray flux sensor. The internal search coil method is invasive, and is not practical in industrial condition monitoring applications.

- *Induced voltage.* When there are broken rotor bars, the voltages induced in the stator windings are affected, providing an indication of faults. However, changes in terms of loads, temperature of rotors, inertia, and supply voltage affect the usefulness of this method (Supangat et al. 2007). In addition, continuous monitoring using this method is deemed impractical, as faults cannot be measured reliably and the method is invasive (Mehrjou et al. 2011).

- *Surge test.* In condition monitoring of stator windings, a surge test can be used. To perform the test, two identical high-voltage, high-frequency pulses are imposed, while grounding is applied to the remaining phase of the motor winding (Thorsen and Dalva 1997). The reflected pulses can detect any insulation faults between the winding and coils. In Huang, Habetler, Harley, and Wiedenbrug's article (2007), the surge test was used to detect eccentricity problems in rotors. The eccentricity problem could lead to an asymmetric air gap. As a result, the shape of the surge waveform is altered in each revolution, which signifies the air gap problem.

- *Motor current analysis.* In this method, the electromagnetic characteristics of an induction motor are measured. By applying a small amount of power, the amplified responses are compared, which in turn allows the rotor and winding conditions to be evaluated (Penrose and Jette 2000). This method is useful for detecting variations from electromagnetic characteristics in the motor. By using a de-energized induction motor, a number of inductance- and resistance-based tests can be performed. The motor conditions can then be accurately evaluated by combining the measurement taken from inductance, impedance, resistance, as well as phase angle (Penrose and Jette 2000).

- *Acoustic emission.* This method can be exploited for detecting rotor and bearing problems. However, the accuracy rate of using acoustic measurements for detecting rotor problems can be compromised in noisy environments (Li and Mechefske, 2006). On the other hand, an ultrasonic wave can be launched for monitoring faults related to stator bars (Lee, Nelson, Scarton, Teng, and Ghannad 1994).

- *Temperature.* A rugged temperature sensor can be mounted on the winding or embedded in the insulation, which is electrically isolated from its instrumentation. Temperature information can be used to study winding insulation degradation.

- *Air-gap torque.* When an induction motor rotates, the current and flux linkages produce an air gap torque. Harmonics of specific frequencies in the air gap torque emerge when the motor is subject to an unbalanced supply (Mehrjou et al. 2011). The air gap torque can be analyzed such that unbalanced stator winding and rotor bar faults can be differentiated (Hsu, Woodson, and Weldon 1992). Nonetheless, it is difficult to measure the air gap torque precisely, or in a direct way (Mehrjou et al. 2011). Owing to the natural frequency of the motor frame, shaft, and rotor, some variations between the measured pulsating torque and the actual air gap torque is expected.

- *Motor current signature analysis (MCSA).* MCSA works by measuring currents from the stators of induction motor. The measured currents are processed to produce their power spectrum profiles. Motor faults can then be detected by analyzing the resulting power spectrum profiles (Siddique et al. 2005). Currents are restricted from flowing through a cracked rotor bar; therefore, no magnetic flux can be sensed from the bar. When asymmetric rotor bars occur, a non-zero backward-rotating field is formed. As a result, harmonics pertaining to the stator winding currents are induced (Mehrjou et al. 2011). In Siau, Graff, Soong, and Ertugrul's article (2004), a formulation to determine the number of broken rotor bars based on stator currents is provided.

- *Partial Discharge.* This is a small electrical discharge that occurs due to insulation imperfection. For example, delamination within the ground wall insulation, resulting from poor manufacturing or overheating, gives rise to voids or air pockets, which get discharged (Tanaka 1995). The partial discharge analyzer test is one of the first techniques to be used during normal machine operation. A deteriorated winding has a partial discharge activity approximately 30 times higher (or more) than a winding in good condition. The effectiveness of stator winding maintenance can be easily monitored with an online partial discharge test (Tetrault, Stone, and Sedding 1999).

- *Gas Analysis.* The degradation of the electrical insulation within a motor produces carbon monoxide gas, which passes into the cooling air circuit and can be detected by an infrared absorption technique (Tanver, Gaydon, and Ward 1986). The high-frequency pulse width-modulation pulses generate excessive voltage peaks leading to the start of motor insulation breakdown. It occurs as a result of electrostatic fields surrounding oppositely polarized conductors that begin to strip electrons from the surrounding air gap, leaving molecules with positive electrical charge (ionization) producing ozone that get combined with nitrogen from the air to produce forms of nitrous oxides. It corrosively attacks the insulation causing embitterment and eventual fracture. Ozone sniffing techniques are used for the detection of ozone.

The data collected using the above-mentioned monitoring techniques are processed either in the time-domain, including computing the root mean square (RMS), mean, standard deviation, and kurtosis of the signals, or in frequency-domain including computing Fast Fourier Transforms (FFT), short-time Fourier transforms (STFT), power spectral density (PSD), and so on. Thee data analysis methods are briefly described below.

3.1.2.1   ***Time Domain Analysis.*** The most common time domain analysis technique currently employed in bearing diagnostics is taking the RMS of various time domain signals, including vibration or accelerometer signals (see Figure 6) and stator currents (see Figure 7). The primary benefit of RMS monitoring is that the measurement can be easily trended over time. The straightforward comparison of the RMS signal to a preset threshold value can indicate a change in machine condition. Appropriate time domain signals that are suitable for bearing fault diagnosis include RMS and kurtosis of the motor current (see Figure 8), as well as the RMS of the vibration signal (see Figure 9).

RMS calculation:

$$\{x_1, x_2, \ldots, x_n\}$$

$$x_{rms} = \sqrt{\frac{1}{N}\sum_{n=1}^{N}[x_n]^2}$$

Kurtosis calculation:

$$k = \frac{\frac{1}{n}\sum_{i=1}^{n}(x_1 - \bar{x})^4}{\left(\frac{1}{n}\sum_{i=1}^{n}(x_1 - \bar{x})^2\right)^2}$$
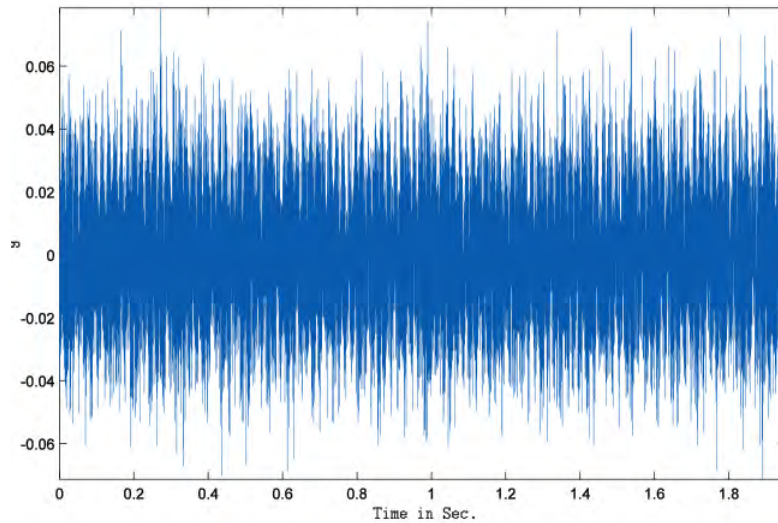

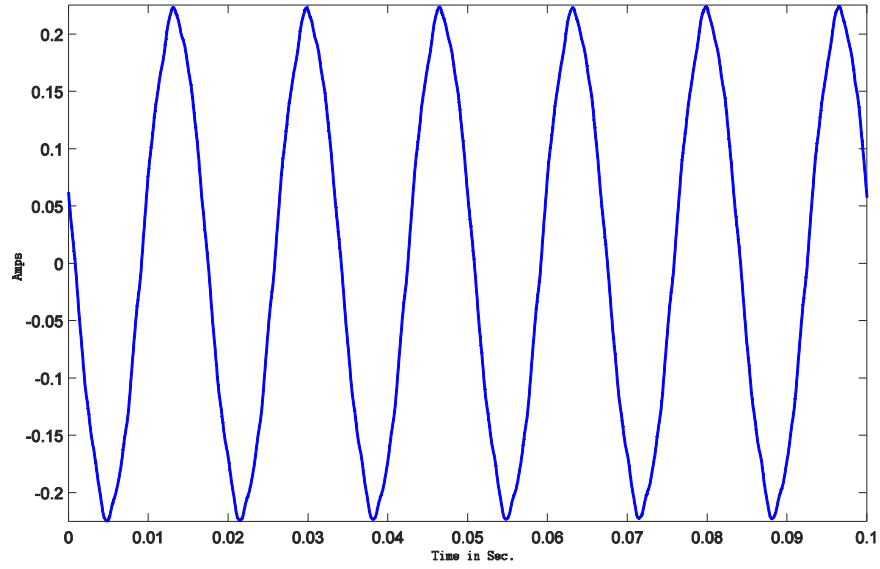Figure 6. Time domain vibration signal accelerometer X-direction (Barbieri et al. 2015).

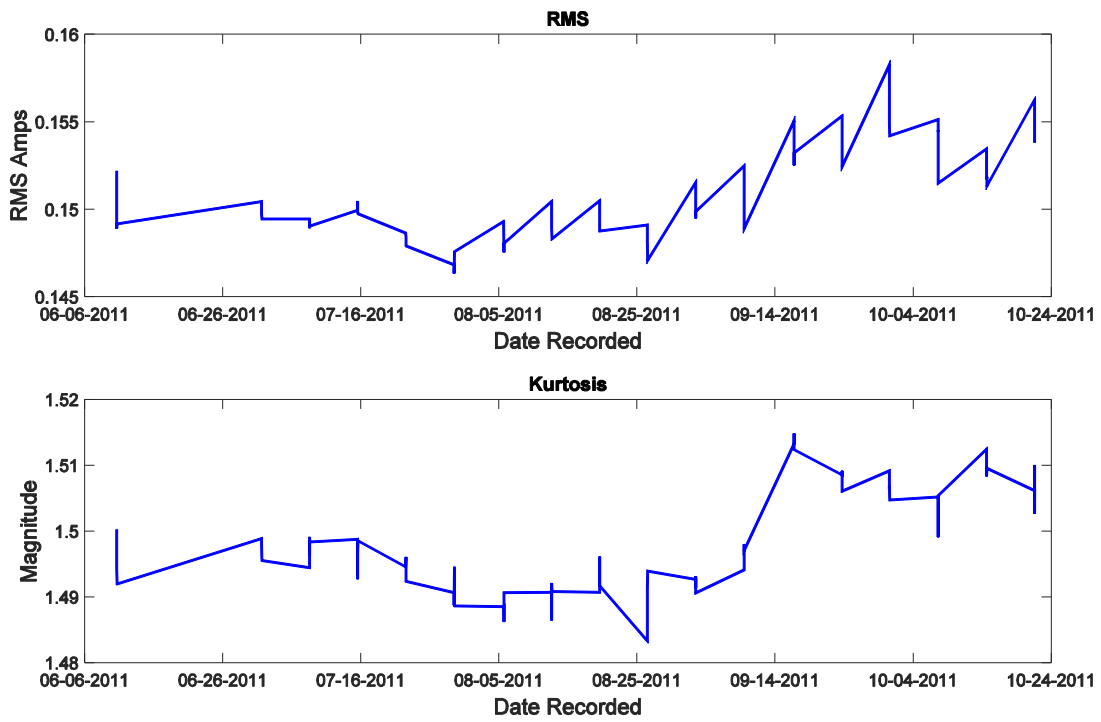Figure 7. Time domain signal of C-Phase motor current (Barbieri et al. 2015).

Figure 8. RMS and Kurtosis of C-Phase motor current signal (Barbieri et al. 2015)
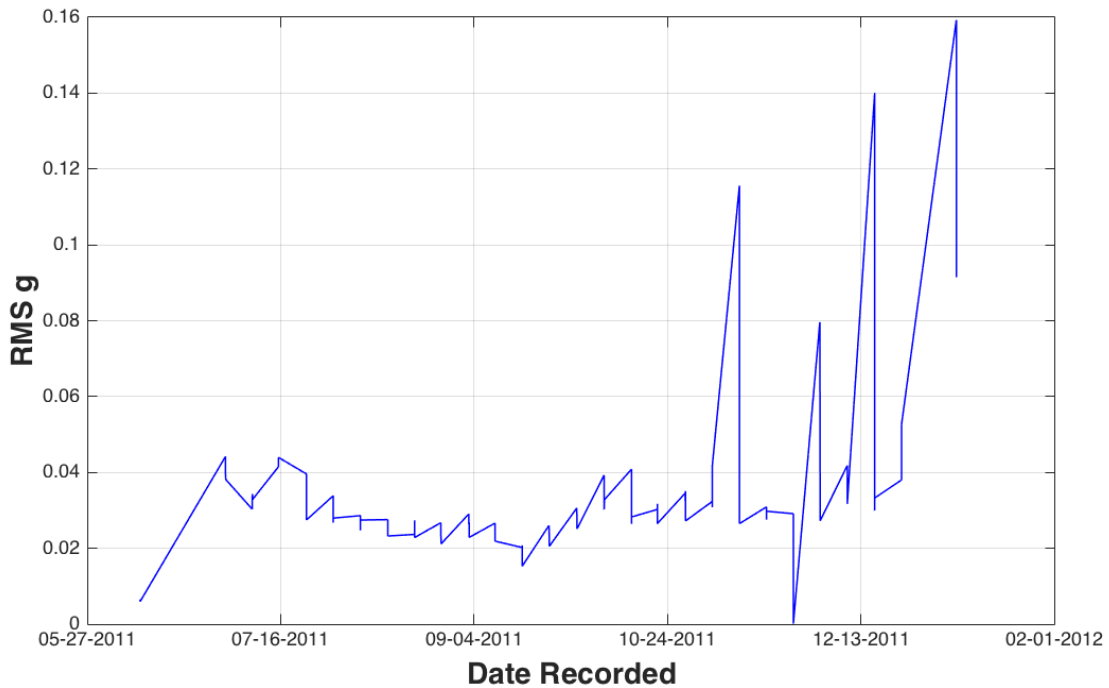
Figure 9. RMS value of motor vibration signal in X-direction (Barbieri et al. 2015).

3.1.2.2   ***Frequency Domain Analysis.*** Many signal features, which may be difficult to identify in the time domain, become significantly simpler to ascertain in the frequency domain. These elements may include vibration due to unbalance misalignment, looseness, and electromagnetic vibration. Frequency analysis may also aid in the detection of non-stationary signals. Probably the most common form of frequency domain analysis is the FFT. Though conventional FFT techniques are capable of capturing discrete bearing defects, many times it is problematic to locate specific bearing faults. These difficulties arise from several origins. First, many fault vibration signatures are amplitude modulated. Second, vibration signals may be buried within other vibrations of the machine, masking the bearing fault. Wavelet Transform and STFT are several methods that may be employed to overcome deficiencies in the FFT. An example of a series of FFT taken from the time series data acquired from an induction motor is given in Figure 10. An additional frequency domain approach to bearing analysis is observing the PSD of the vibration signal (see Figure 11). The PSD for a given machine can be archived over time for trend evaluation.

Frequency Domain Transforms

Fast Fourier Transform calculation:

$$FFT\ X(k) = \sum_{j=1}^{N} x(j)\omega_N^{(j-1)(k-1)}$$

Power Spectral Density calculation:

$$PSD\left(\bar{x}_n^2\right) = \frac{P_{xx}[i]CG^2}{NGf_{bin}}$$

Where:

$$Coherent\ Gain\ (CG) = \frac{1}{N}\sum_{i=0}^{N-1}\omega[i]$$

$$Noise\ Gain\ (NG) = \frac{1}{N}\sum_{i=0}^{N-1}\omega[i]^2$$

$$Frequency\ bin\ (f_{bin}) = \frac{1}{N(time\ sample)}$$

$$P_{xx}[i] = \bar{x}_n^2\left(\frac{NG \cdot f_{bin}}{CG^2}\right)$$
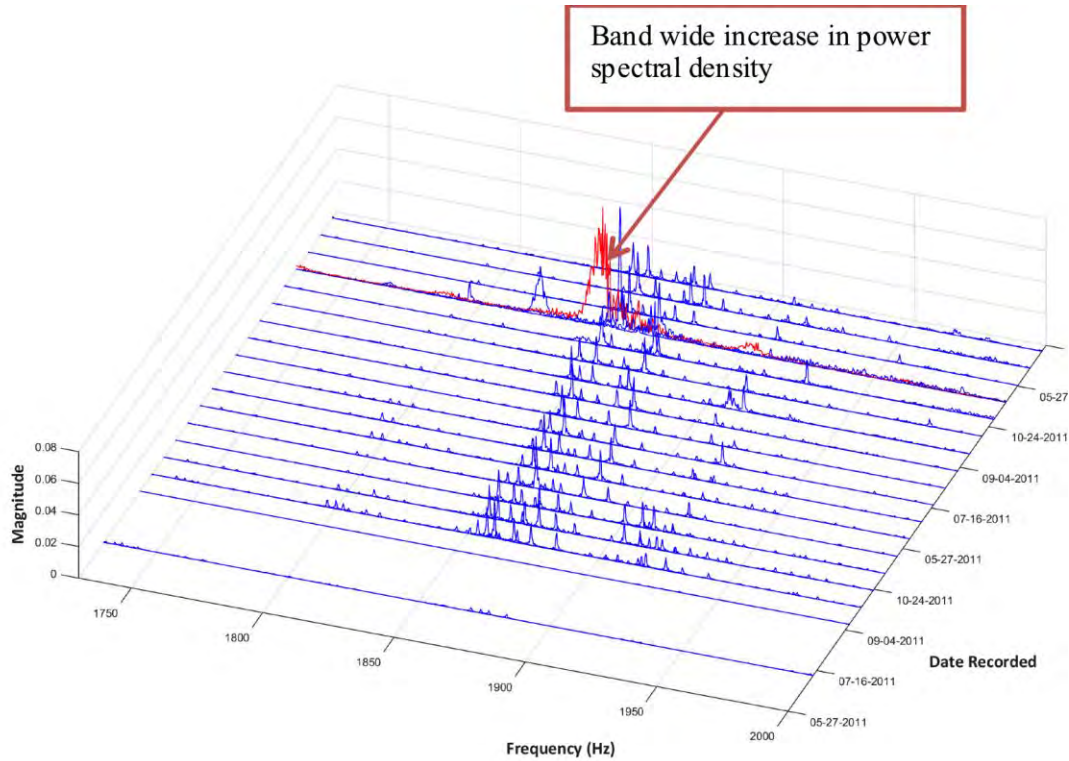
Figure 10. FFT of motor vibration signal in X-direction (Barbieri et al. 2015).
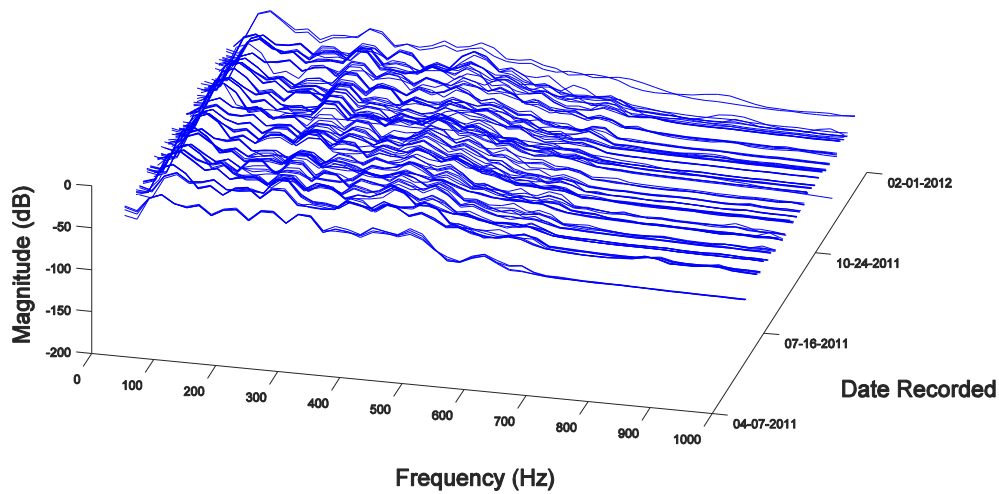
Figure 11. PSD of motor vibration signal in X-direction (Barbieri et al. 2015).

3.1.3   Fault Signatures

The steps described in EPRI (2012) are followed here to develop diagnostic fault signature information for large induction motors. As defined in (EPRI 2012), a fault signature is a structured representation of the information that an expert would use to first detect and then verify the occurrence of a specific type of fault. A fault describes a particular mode of degradation that can be detected by analysis of plant information before the asset condition reaches the point of failure to meet a service requirement. Implied is an assumption that the fault is detectable by analysis of plant information and that the analysis can be performed in time to prevent or otherwise remedy the fault condition before it becomes a failure condition.

A fault signature has three information attributes: Asset Type, Fault Type, and Fault Features, as shown in Figure 12. The steps followed to populate the AFS database with different fault signatures are shown in Figure 13.

During the content development exercise several such technical examinations were created for implementation in the FW-PHM Suite they include:

- Temperature (RMS)
- Vibration (RMS)
- Vibration (Frequency Harmonics)
- Electrical current (RMS)
- Electrical current (Kurtosis)
- Electrical current (Frequency Harmonics)
- Acoustic input.

However, EPRI AFS Database has additional technical examinations already implemented as part of their master database.
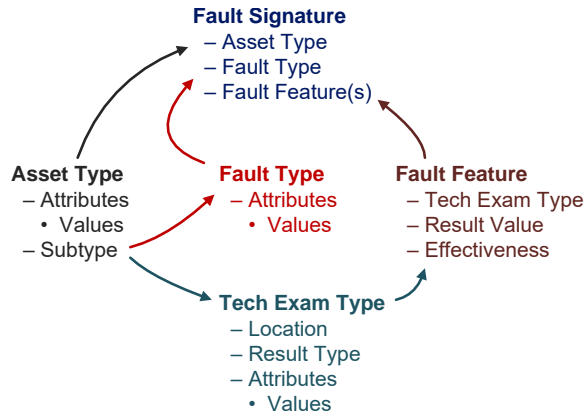
Figure 12. Different attributes of fault signature (EPRI 2012).
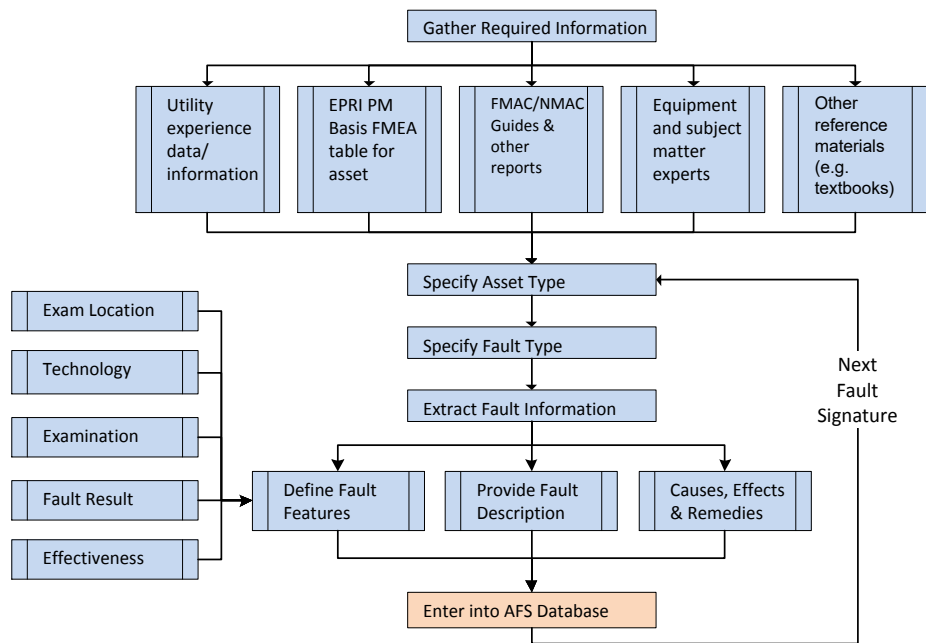
Figure 13. Steps involved in gather faults signatures (EPRI 2012).

4. VALIDATION OF FAULT SIGNATURES

Three data sources were studied to examine or update the implementation of diagnostic models (fault signatures) in the FW-PHM Suite. The first set includes accelerated degradation data collected in experiments run at The University of Tennessee, Knoxville (UTK), in which bearings in small induction motors were stressed due to aggressive heat and humidity exposure. The second set is a practical example from INL's Advanced Test Reactor (ATR) where vibration data is collected on operating systems periodically and examined by a subject matter expert (SME) for signs of degradation and need for maintenance, repair, or replacement of motors. Due to the fact that the first two data sets did not provide specific signatures and reliable trends for development of RUL models, a validation platform was constructed in cooperation with Idaho State University's Energy Systems Technology and Education Center (ESTEC) with two medium-sized induction motors on which degradation experiments was performed.

4.1 University of Tennessee, Knoxville Experiment

The UTK data was collected on ten 5-HP US Electrical 3-phase induction motors that were subjected to degradation (end of life) testing through aggressive heat and humidity exposure (Barbieri, Hines, Sharp, and Venturini 2015). In an attempt to capture the effect of differing amounts of stress, the ten motors were divided into two subgroups. Group "A" contained seven motors subjected to 160°C heating via a convection oven. Following the heating cycle the motors were exposed to a high-moisture degradation bed for additional stress and corrosion. The remaining three motors were subjected to 140°C heating via a convention oven and then were exposed to a high-moisture degradation bed. The entire degradation process was carried out over the period of 1 week for both the motor groups.

Following the degradation process, the motors were moved to a test bed where data was collected from each of the motors under full load conditions at a sampling rate of 10240 Hz. Full load conditions were achieved by coupling each of the motors to a generator, which was in turn connected to a load bank. The motors were allowed to run for 1 hour with data being collected in 15-minute intervals for 2 seconds. Thirteen signals were collected from each of the motors, they include:

- Input current (Phase A, Phase B, and Phase C)

- Input voltage (Phase A, Phase B, and Phase C)

- Accelerometer (X–direction and Y–direction)

- Tachometer

- Microphone

- Temperature

- Output voltage and current.

4.1.1 Bearing Failure

While motor failures can be produced by faults in many different motor components, five out of the ten test motors experienced failures directly related to bearings. Since this report focuses on bearing failure, the experience related to bearing failure is discussed here.

The FFT or PSD of each of the raw data signals were calculated and peaks within particular frequency ranges were tracked by a series of scalar values over the history of the motor. Figure 14 depicts the tracked peak values of the vibration signals in the X-direction for Motors 1 and 2 over the specific bandwidth of 1730–2000 Hz, with a threshold cut off value of .04 for anomaly detection. To create a RUL model based on peak value tracking would involve curve fitting the measured data and forecasting the expected time of failure when the peak value would exceed the operational threshold limit. Perhaps some conservative method of estimating the RUL based on this threshold and the current trend (e.g., value and slope) exists; however, a straightforward trend given this data set was not observed. For example in Figure 15, the signal approaches close to the threshold many times suggesting a short RUL before settling down for a long period of time prior to climbing through that threshold at the point of motor failure. These results do not provide a transparent measure of RUL that provides any high value to operational decisions based on implied longevity expectations.
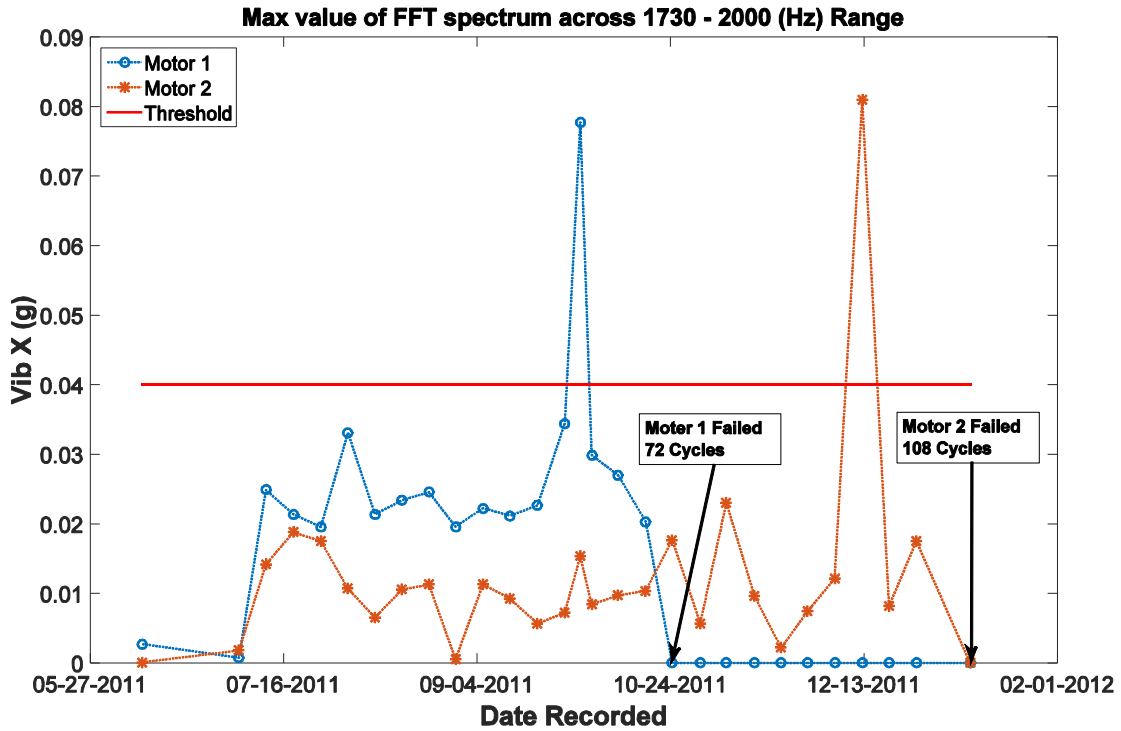
Figure 14. Trend of maximum amplitude of vibration frequency spectrum for Motors 1 and 2.
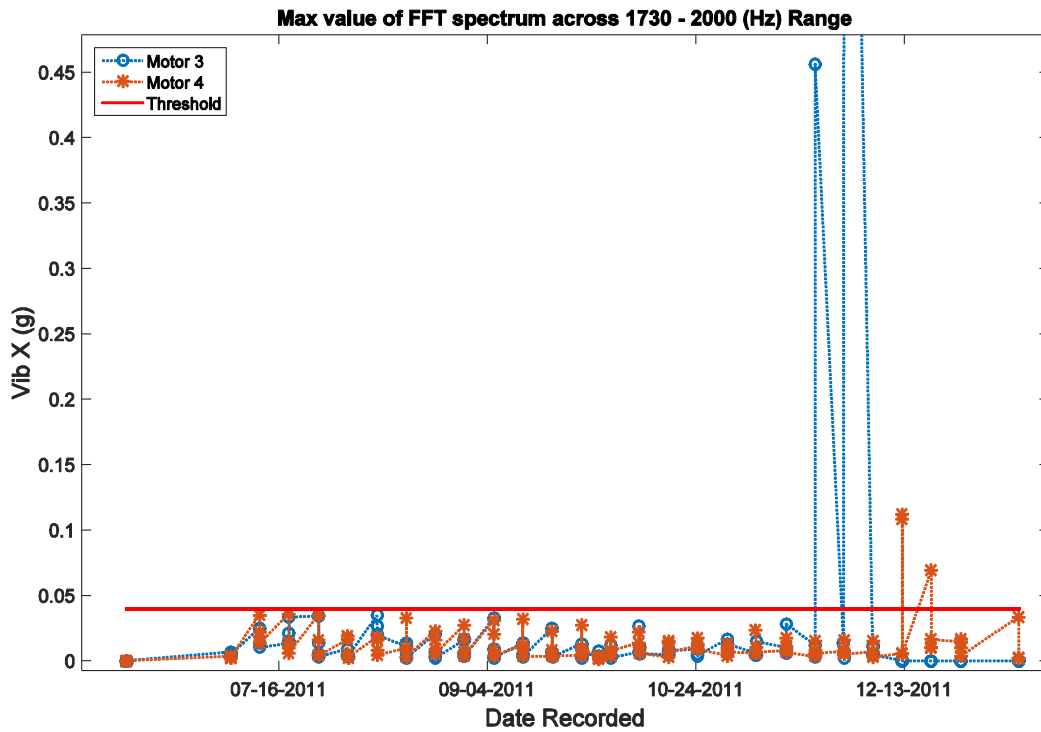

Figure 15. Trend of maximum amplitude of vibration frequency spectrum for Motors 3 and 4.

4.2   INL ATR Operational Data

In another effort to develop fault signatures associated with bearing faults using vibration signals, data from INL's ATR facility were investigated. The motors at ATR are coupled to a mechanical system within the pumping systems. Vibration sensors are placed in several locations shown in Figure 16. A technician acquires data periodically. A SME who is trained to interpret data and make diagnoses of conditions that require attention, then analyzes the data.
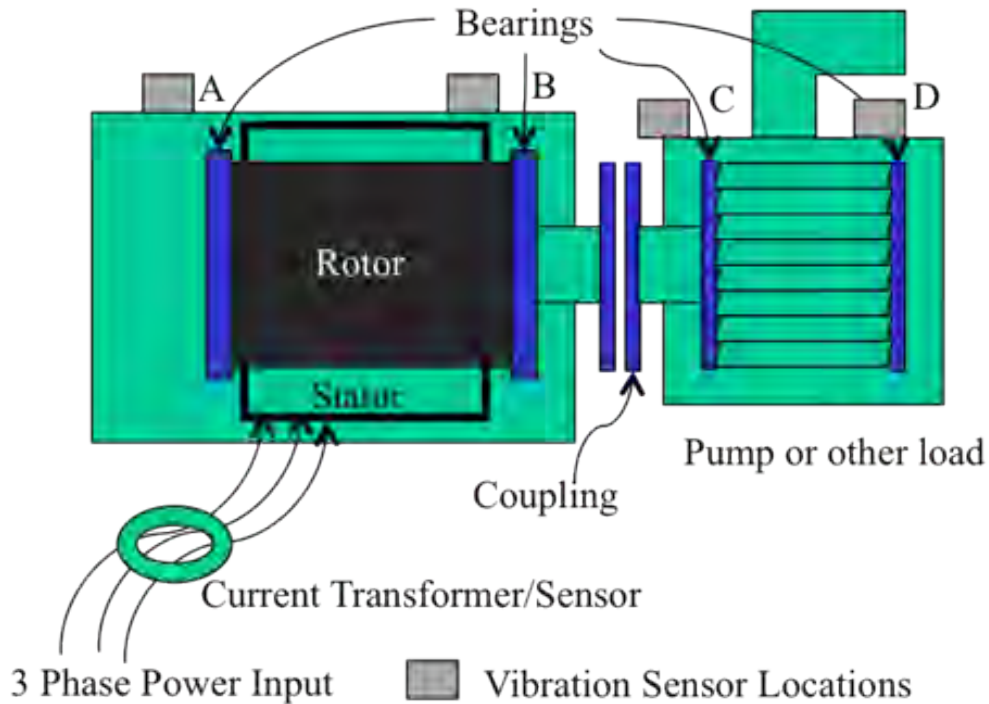
Figure 16. Diagram of motor and pump with vibration sensor locations indicated as A, B, C, and D.

The analysis proceeds with the SME surveying data for preconfigured thresholds, and continues with the SME observing trends that may show a strong deviation from the previous reading history. Examining frequency spectra of the signal that may indicate specific fault signature may follow a process of analyzing the most consolidated data, like RMS value of the vibration amplitude.

Some of the challenges associated with scheduling technical examinations for operating pumps periodically include redundant systems. Some systems are not in operation during exam periods. This leads to an asynchronous set of data with respect to snapshots in time, making it difficult to find data sets that establish trends for use in prognostics and RUL development. Online monitoring would be potentially very beneficial to the process of detecting degradation over time. These data sets serve the purpose of applying technical examinations to diagnostics in FW-PHM. The SEM could easily enter the technical examinations and be aided by the signatures entered into the FW-PHM AFS Database.

4.3   INDUCTION MOTOR FAULT VALIDATION PLATFORM

In addition to using publicly available induction motor datasets, INL collaborated with ISU's ESTEC to perform an experimental study to collect data on 40-HP induction motor failures due to bearing faults. The experiment was performed on two identical 40-HP induction motors with one serving as a baseline and the other subjected to bearing degradation scenarios and be rebuilt between experiments. Both the 40-HP induction motors (Model WWE40-18-324T, 480 V, 46.0 Amps, 3-phase, 1775 RPM at 60 Hz) were instrumented to measure stator current on each of the three phases of the motor and vibration in

three axes. The motor instrumentation as shown in Figure 17 included two Allen-Bradley Programmable Logic Controllers (PLCs) to continuously record (1) RMS value of voltage and current from the three phases of the motor, (2) vibration signals, and (3) motor housing temperature (using thermocouples). The sensor specifications are:

- Current transformer (CT): RISH CT 12G458 5 amps to 50 amps into 0.25-ohm burden transformer to convert to voltage

- Vibration: IMI Sensor 640B01, output 4–20 mA signal converted to a 1 V to 5 V signal appropriate for 250 KOhm

- Thermocouple: Rosemount transmitter model 248HANAAA2G3 for sensor PT100_385_4_wire.
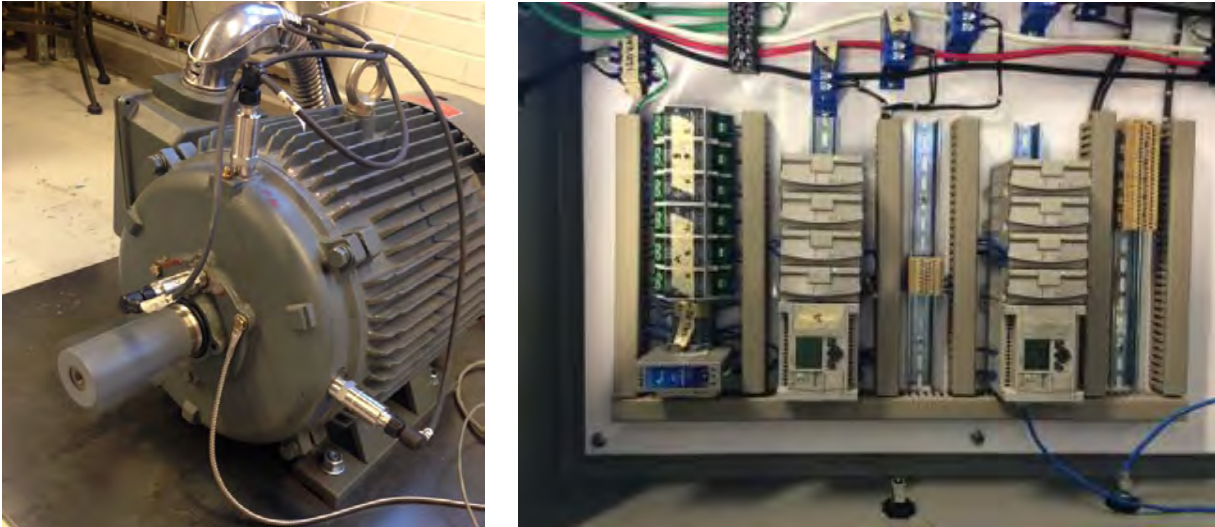
Figure 17. One of the two induction motors with instrumentation (temperature and vibration sensors) and data acquisition system.

Current transformers were used to acquire time varying current signals. The PLC was coded to perform a safety shutdown of the system when temperature or vibration measurements exceeded a predefined threshold value. A NI PCIe-6343 Data Acquisition (DAQ) board with two SCB-68A connector blocks was used to acquire data at fixed time interval at 10 KHz. Each connector block collected signals from one motor, including the three phases of stator current, three axes of vibration, and temperature. A Lab VIEW code is used to acquire time series data at configurable intervals. The sampling rate of 10 KHz allowed sufficient bandwidth to capture all harmonics produced by fault signature with sufficient binning when FFTs are applied. Initially, the program was configured to collect data every 15 minutes.

Initial data sets showed large noise variation in the 4–20 mA signals from the temperature and vibration transducers during baseline data acquisition. Figure 18 shows a measure of the noise in the RMS value of the vibration sensor and the RMS value of the signal after the noise was corrected by grounding the unused inputs to the PLC.

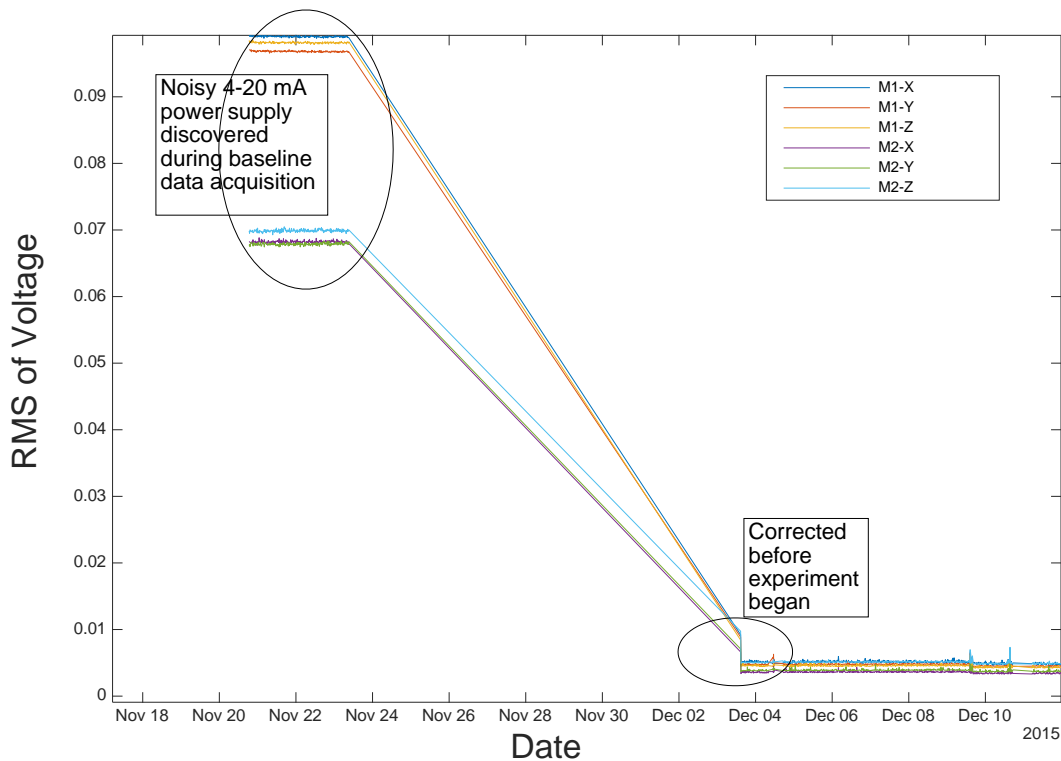Figure 18. Baseline acquisition and beginning of test data from different motor vibration channels showing unacceptable noise that was reduced to acceptable level before experiment was initiated.

4.3.1   First Experiment to Bearing Failure

An initial experiment to failure of the motor bearing was completed during September 2015. This section describes that experiment and the lessons learned that informed the subsequent experiment.

After completing the installation of the two motors and acquiring baseline data sets with stator voltage and current from the installed microcontrollers, one motor, referred as M1, was left unaltered to produce control or baseline data. A second motor, referred as M2, was altered to add a second port to the front bearing that could be opened to allow bearing grease to seep or be flushed out. The standard bearing lubricant port was available to push grease, solvents, or contaminants into the motor. The motors have been run with no external load to date.

By opening the grease drain port in M2. loss of bearing lubrication experiment was initiated. Surprisingly, after 28 hours of operation, M2 bearing showed no signs of degradation. The hypothesis associated with this unexpected behavior is that the motor is unloaded and could be fully supported on the back bearing. Removal of viscous grease actually decreased the torque on the motor. but no significant wear was achieved. As a next step, to ensure grease was removed, light oil and then a solvent was applied through the bearing. The drive current still remained within the normal range for over 12 hours of operation. At this stage, 50 ml of iron fillings were introduced into the bearing. The motor was operated until a highly worn bearing finally created enough friction to cause the torque and current to spike to the trip set point. Figure 19 shows the RMS value of drive current collected by the PLC. Figure 19 illustrates a sudden spike in the RMS value of the drive current. The spike occurred after iron fillings were added to the motor bearing. At this point, the system tripped automatically. The dissembled motor is shown in Figure 20. From Figure 20, one can observe the level of damage that occurred to the rotor winding and motor internal due to the presence of contaminants in the bearing. The important lesson learned here is

19

that one faulty condition can (unintentionally) add to another in a relatively short period of time. Also, during the initial experiments, only current data was collected and no vibration data was available. Continuous temperature data was also not collected; however, periodic thermal images of the motor were collected using a hand-held thermal camera.
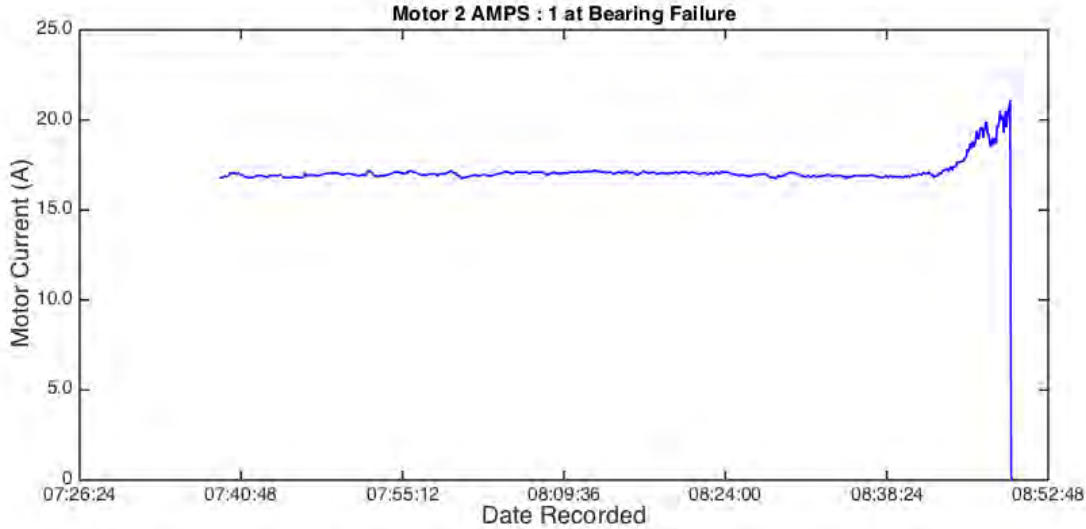

Figure 19. Phase A motor current of M2 after introduction of iron filing contaminant.

Figure 20. Selected portions of dissembled motor after loss of bearing lubrication and presence of contaminant test.

4.3.2   Second Experiment to Bearing Failure

A second experiment was constructed with an objective to attempt a more gradual bearing degradation. After replacing the worn bearing and reassembling the motor, the grease was drained and flushed over an approximately 72-hour period. The back bearing was not replaced before this experiment, as it was not degraded during first experiment. The list of steps followed to collect key data sets obtained are given in the following:

- Baseline – reconditioned motor with bearing replaced

- Lubrication gravity drain (LD)

- Air forced completion of drain (LFD)

- Degraded operation after force drain (DO)

- Replaced lubrication through the port (RL).

The sensors were updated to include current transformer with a burden resistor that allowed a voltage representation of the drive current, a set of vibration sensors, and a thermocouple mounted on the motor bushing. As before the RMS, current data reveals very little change; however, the frequency spectra did reveal changes in the character of the data sets. The frequency spectrum above the fundamental of the unaltered motor (Figure 21) shows the harmonics similar to those predicted by (Benbouzid 1999) for the unloaded motor. The ratio of the peak magnitude at the 7th harmonic of 60Hz (420Hz) to the peak magnitude at the 5th harmonic (300Hz) is slightly less than one. By observing the progression over the duration of the grease removal process, the dominant amplitude at these two frequencies is shown to reduce in Figure 22.
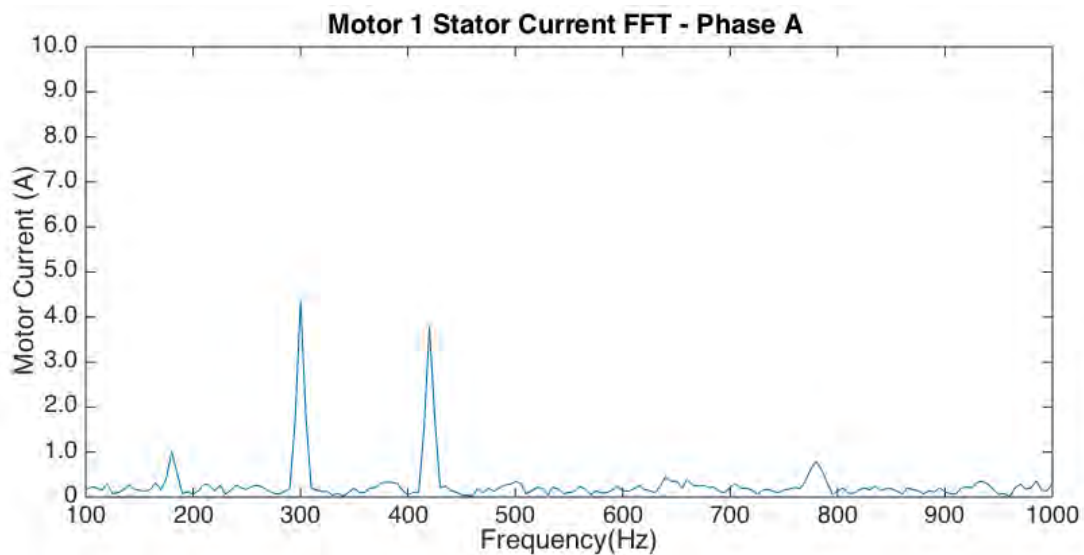

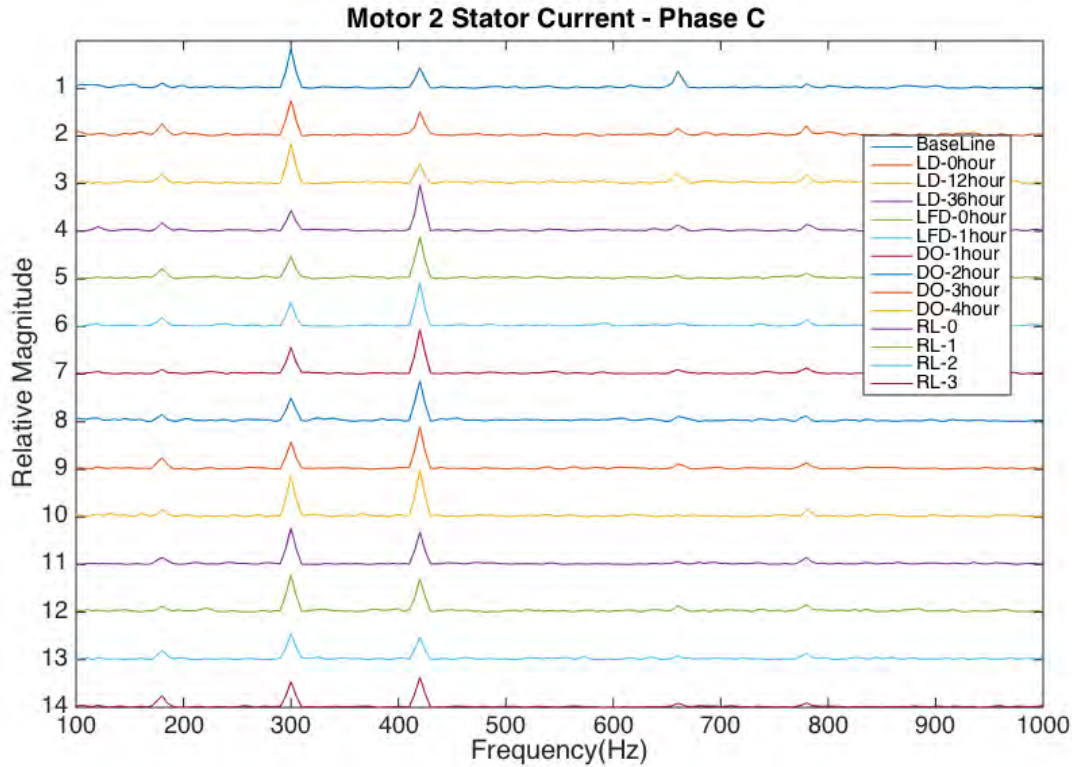Figure 21. Baseline frequency spectrum from the unaltered motor M1.

Figure 22. Frequency spectra of M2 at different steps of the second experiment.

The lubrication drain process yielded a measurable change in $7^{th}/5^{th}$ harmonic amplitude by the end of the natural drain cycle completion. However, completion of drain by forced air (i.e., LFD) did not increase this ratio further and no other obvious indicators were observed. On the other hand, the ratio decreased somewhat through the duration of the test even though acoustic from the motor increased enough that after 4 hours of operation the decision was made to shutdown the test and reintroduce lubrication through the grease port. After reintroduction of grease, the motor was restarted and the sound level decreased to pre-drain level with the harmonic amplitude ratio decreasing to below 1. The trends of the individual harmonics and the ratio are shown in Figure 23. For sake of convenience and better representation of trends, the ratio value was scaled by 100. The other two phases of current show similar trends.

Unfortunately, the vibration sensors were not effective in showing the trauma that the audible noise level was indicating, and audio was not captured in a systematic method. Temperature did increase over the duration of the test but was not indicative of onset of the degradation that would be necessary for effective RUL determination. Based on these results, several instrumentation improvements were identified for the next set of tests. First, vibration sensors that are sensitive enough to provide the accelerations that were obviously occurring needed be installed, positioned, and tested for sensitivity prior to another experiment. Data collection of the sample rates adequate for frequency domain analysis needed be automated to take regular and frequent samples, with a data acquisition system that does not depend on human operation of an oscilloscope. It is possible that a clear trend between the second and third sample of lubricant drain would give clear usable information for derivation of RUL. Finally, the bandwidth of the signal collection needed to be increased to produce better resolution in the frequency domain.
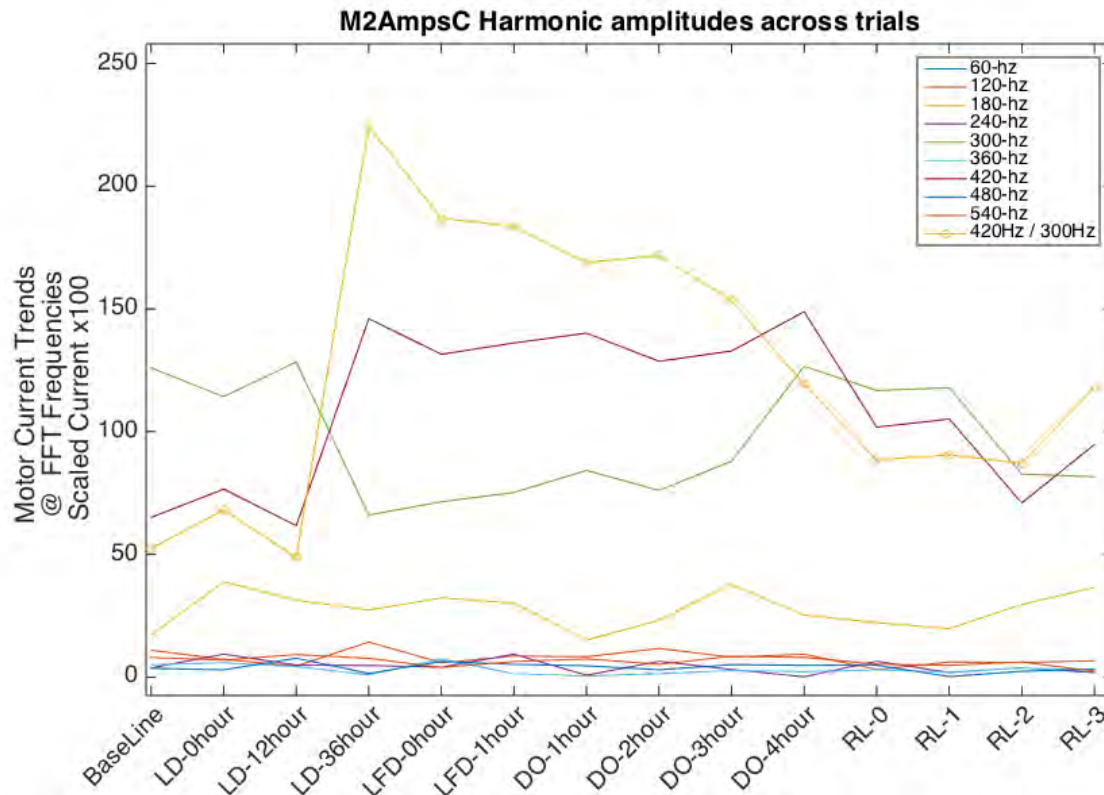
Figure 23. Trends of the drive current frequency harmonics over the duration of the removal/replacement process of the second experiment.

4.3.3 Third Experiment to Significant Bearing Degradation

The lessons learned were applied to a repeat of the loss of bearing lubrication experiment. The motor rebuild with new front and back bearings and improved instrumentation was completed and tested by the end of November 2015. As before, the unaltered motor (M1) and experimental motor (M2) were run to obtain and operational baseline. M1 was run continuously such that a comparison could be made in the same electrical and environmental conditions. The decision was made to run the motors over an extended period of time continuously so that gradual degradation evident is observed in the data. Figure 24 shows an annotated data graph to provide a timeline for the experiment activities.

The experiment followed this path:

1. Baseline with motors running data acquired November 20–23, 2015

   a. Discovery of large noise source in the 4–20 mA data signals caused by power supply noise and ungrounded inputs to PLC leading to ground loops.

   b. Resolved with grounding of unused inputs and filter capacitors on power supply

2. Baseline noise level acquisition with motors not running prior to starting experiment

3. Remove bearing grease drain plug removed December 4 with intent to run until degradation was obvious

   a. M2 was run continuously until December 30

   b. M1 was momentarily shutdown to acquire a data set with only M2 running to confirm acquisition channels were correctly assigned—restarted after confirmation

23

c. Power failure during ESTEC holiday break cause continuous test to be disrupted

d. Restarted on January 4

4. Team made the decision to take additional action to induce visible degradation and flush the bearing if no change was observed; motors were stopped to make these adjustments January 13

a. Removal of bearing cover showed that grease remaining in the chamber was being drawn up into the bearing, thus effectively lubricating the bearing

b. All remaining grease was manually removed to leave a completely unpacked bearing

5. Motor was restarted with unpacked bearing January 13 for a 12-hour run.

a. Data acquisition frequency changed to 1-minute intervals anticipating possibility of rapid changes

b. No changes were observed by operators

c. Next step to flush with Harbor Freight "air tool oil" (similar in weight to 15W-40 oil) was taken but filling through grease fitting and draining through plug.

6. Motors run for 15 minutes

a. No changes observed

b. Next step was to flush light lubricant oil out with solvent

7. Motors run with bearing flushed until January 15

a. No changes observed by operators

b. Decision to introduce iron filings was made

8. Contaminant test

a. Immediate effects observed.

b. Spike in current followed by increase in vibration signal

c. Operator reported very audible noise to INL

d. INL advised to discontinue test before additional damage that may result in more complicated rebuild occurred

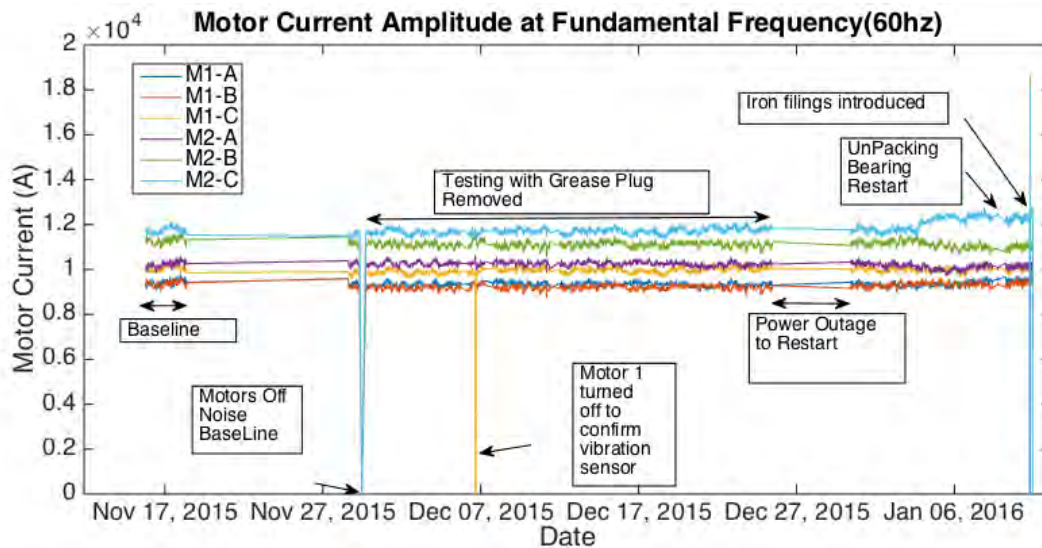9. Test terminated January 15 at 10:56 pm.

Figure 24. The timeline of the extended bearing test is summarized in the annotation for the motor current plot.

Data was acquired at 15-minute intervals for the bulk of the test. Time series data was acquired at 80 KHz for the six current and six vibration measurements at each sampling interval. The files were named with the time stamp of the sampling interval. Files were transferred from the acquisition machine intermittently to a cloud storage resource for processing at INL. A MATLAB® script was written to apply a series of standard processing steps to each file and enable graphs to be generated easily processed files. Processing steps:

1. Find the mean of the time series

2. Find the root mean square of the time series

3. Apply a hamming window the time series adjusted by the mean to avoid square window high frequency affects (Figure 25).
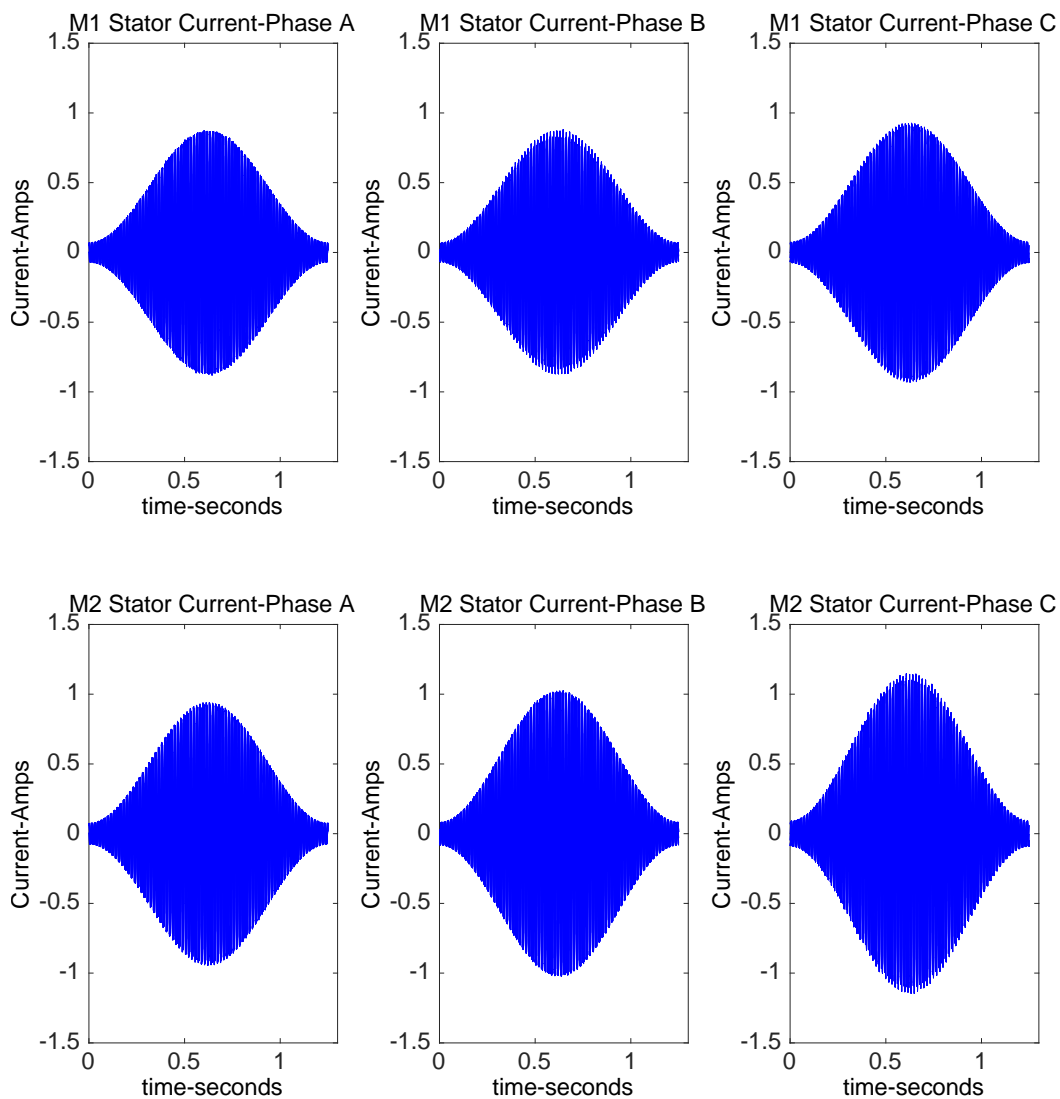
4. Calculate the Fast Fourier Transform (Figure 26).

Figure 25. Examples of time series data after subtracting mean and applying a hamming window. Three phases of current data for each motor shown with M1 on the top and M2 on the bottom row.
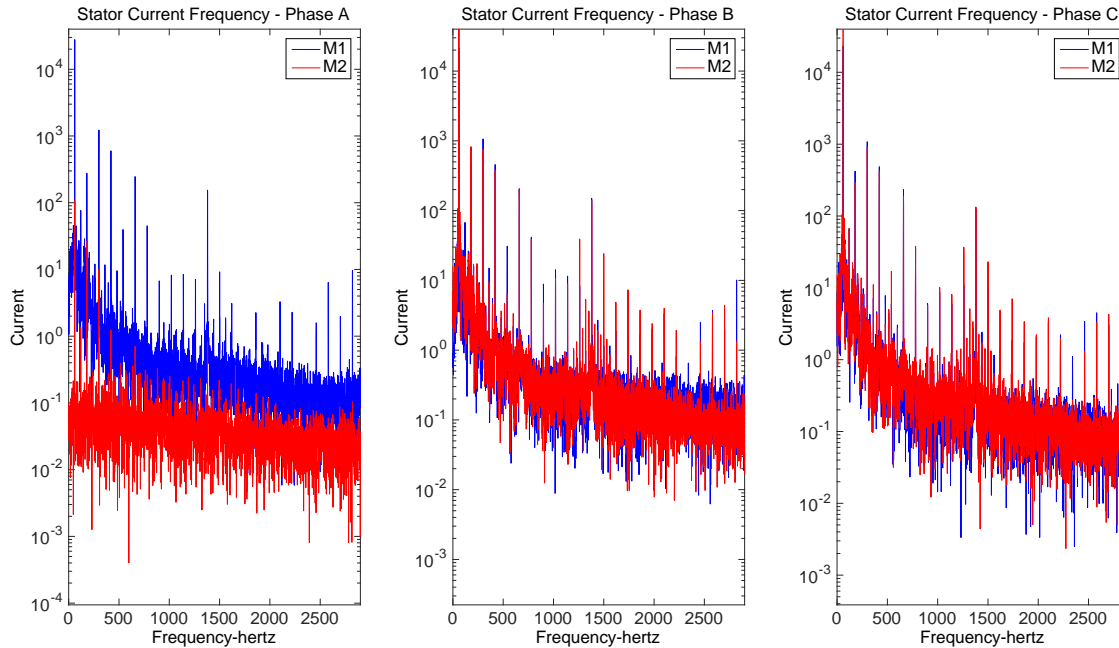
Figure 26. FFT of current example showing M1 in blue and M2 in red.

In Figure 26, blue is most visible in the left plot is because this was the result of the immediate introduction of the contaminants showing Phase A for the M1 current dropping low and Phase B and C increasing dramatically. The effects of the experiment on the amplitude of the fundamental frequency of the current are summarized in the timeline seen in Figure 24. It is observable that very little change occurs in the overall current signature during the extended gravity drain experiment. Observation of the FFT from beginning to end also shows very little in the relative magnitude change in the harmonic multiples of the fundamental. Near the end of the gravity drain experiment, after the restart, small but observable changes in the currents measure occur where Phase C increases and Phase B decreases. The unbalanced change may be indicative of an issue with the integrity of the windings. The cause is currently still under investigation by ESTEC. An impendence check of the motor in static condition as well as a rebuild baseline after replacing the bearing need to be done to determine if this is the cause, or if some other mechanical signature may be present due to bearing degradation. There is no detectable change in the vibration data at this same stage (Figure 27).

Examining the vibration RMS values as the experiment continued to the unpacking of the bearing, the amplitude of the vibrations is noticeably higher periodically for about 12 hours, followed by a settling to smaller vibrational variations from sample to sample (Figure 28). This corresponds to the 12-hour period the motor was run with the unpacked bearing before flushing with light lubricant and solvent. The motor ran more smoothly with a completely flushed bearing than with an unpacked bearing.
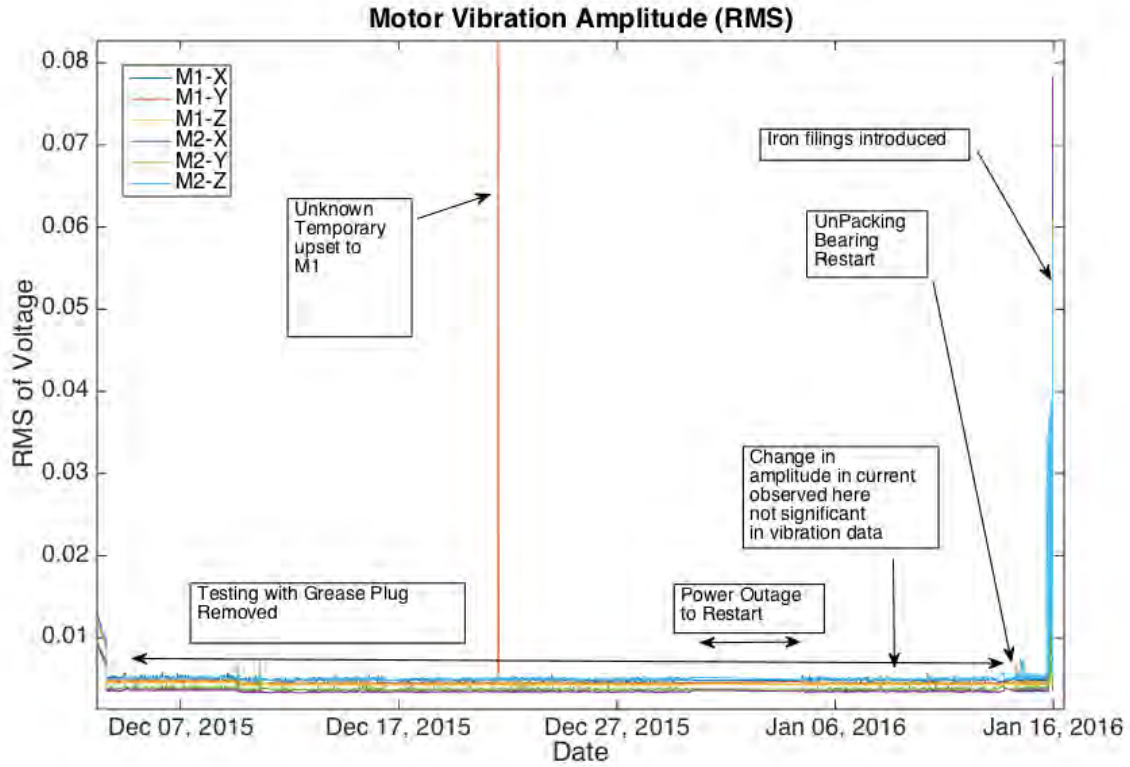
Figure 27. Overview of the vibration RMS data.
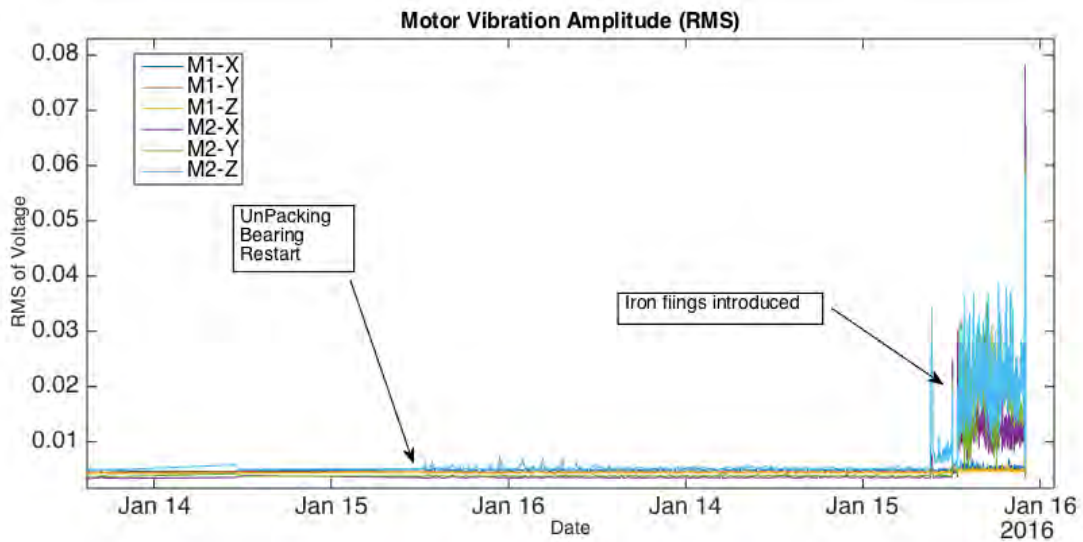
Figure 28. Detailed of unpacking of bearing to end of experiment vibration data.

The fundamental frequency amplitude of Phase C increase at the restart prior to introduction of the contaminants, as seen Figure 29, and does not decrease until the end of the experiment. The moment of the introduction of the contaminant does introduce a transient, but the current quickly settles back to that baseline, indicating the overall torque does not change at steady state for the contaminant test.

27

Figure 29. Detailed of iron filling introduction to completion of experiment.

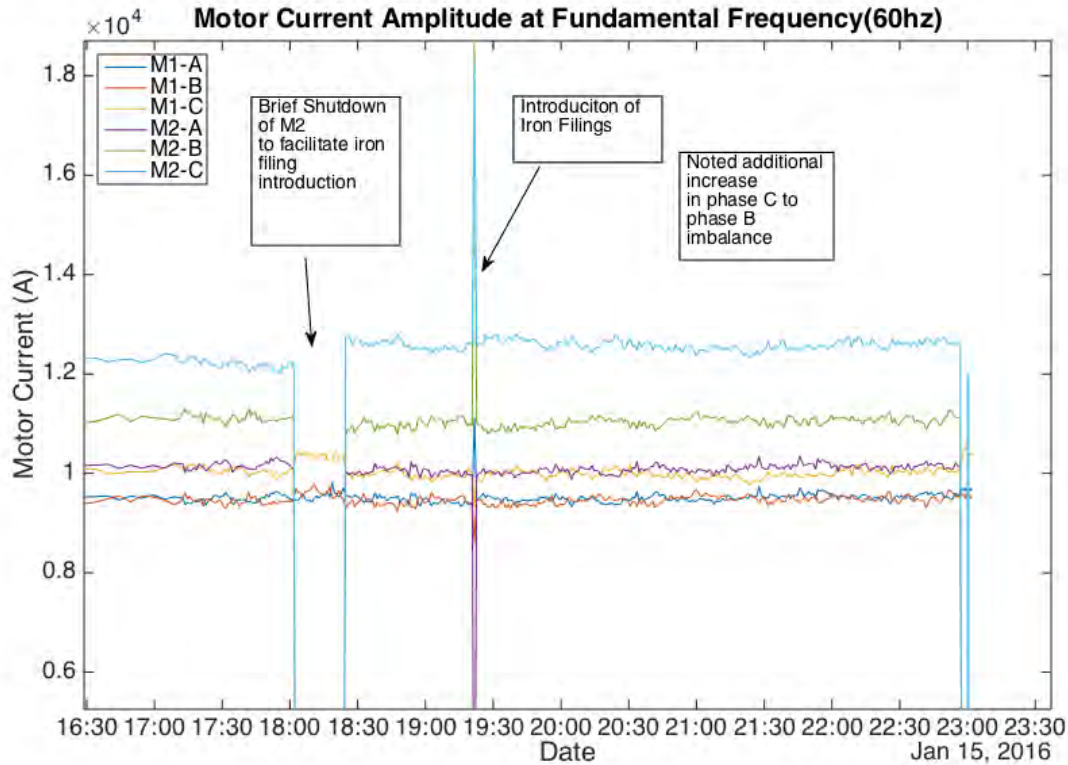The experiments also show that for degradation that is related to the condition of the bearing, the vibration sensors provide a better feedback mechanism for diagnostics, since the current signatures do not show any changes as the bearing lubrication health degrades. For completeness, the difference in the time series of the vibration sensor between the start of the experiment and the introduction of iron fillings is displayed in Figures 30 and 31. The vibration FFT is shown for the introduction of iron filings in Figure 32 to illustrate another instrumentation finding about vibration sensors with 4–20 mA rating. The frequency response of 4-20 mA vibration sensor was not sensitive past the 2nd harmonic. To perform technical exams with frequency specific signatures, voltage-based vibration sensors should purchased to replace the 4–20 mA sensors.
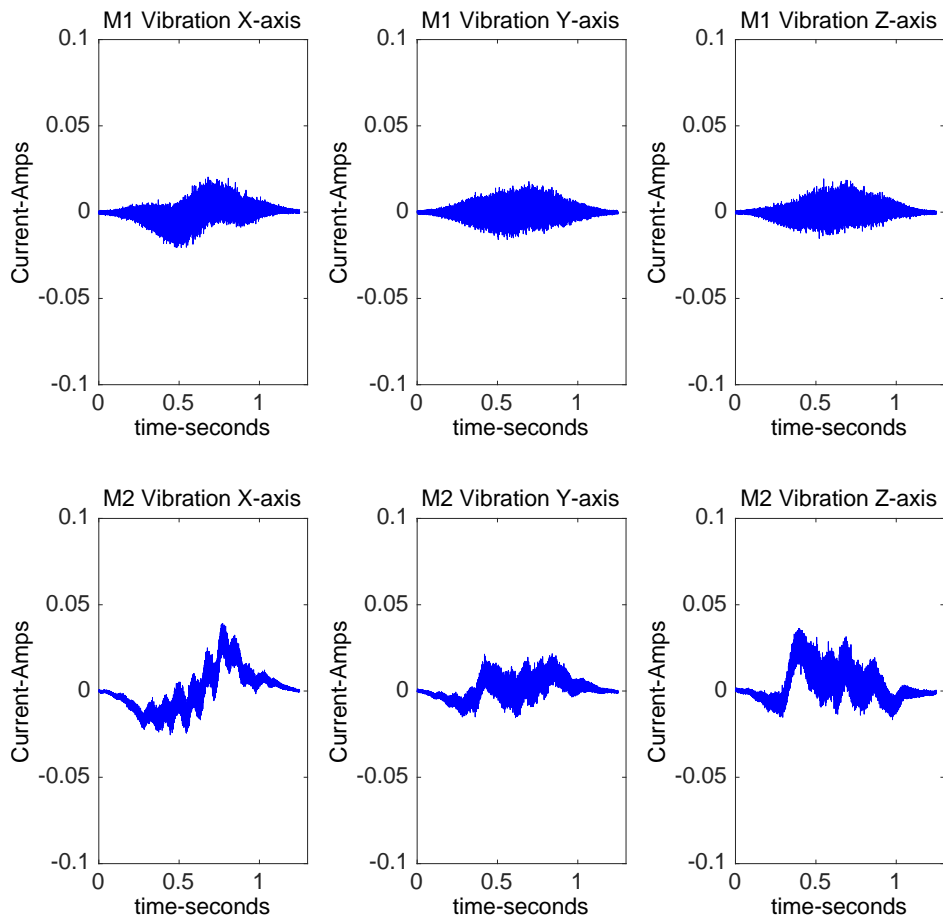
Figure 30. Vibration time series at the introduction of the iron fillings with hamming window.
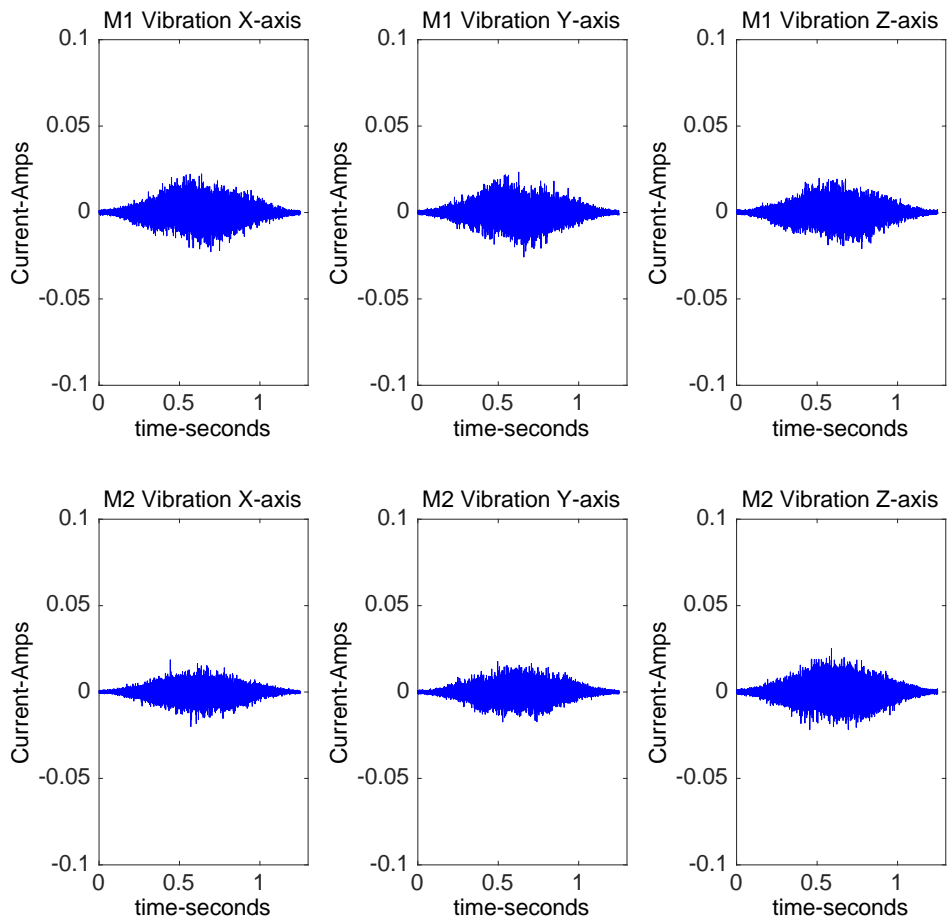
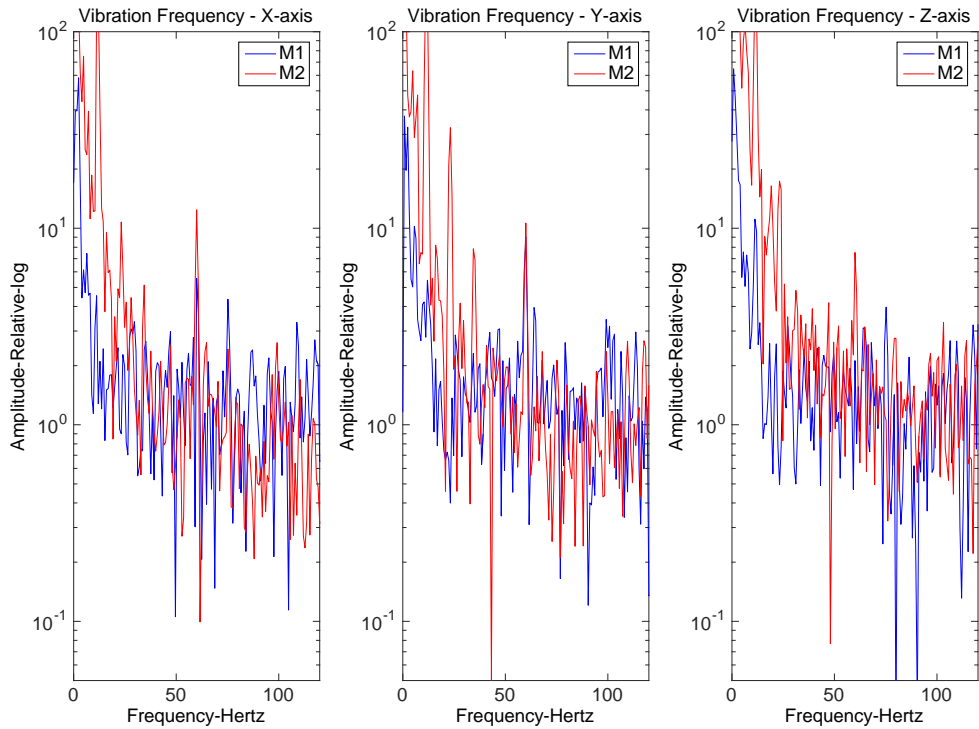Figure 31. Vibration time series during baseline with hamming window.

Figure 32. Vibration FFT after introduction of iron fillings.

A final observation about the current sensors, the observed data is indicating that a degredation may be occuring in the windings of M2. The motor has shown an imbalance between phases greater than M1 since returning to service after the rebuild. Over time the imbalance increased. The balance increased immediately after the last inrush current applied at the restart of the motor after preparation for introduction of the iron filings. This may be the best possibility of a measure of a degradade property of the motor that is growing over time, even though this was not the intended target. This effect could be due to abuse suffered during the first dramatic test that was continued to degrade with use. The root cause will need to be determined to understand the validity of this measure of the health of the motor and the test continued to understand if a trend exists for which a successful example of RUL can be formed from on-line monitoring of induction motors. For completeness, the lack of variation between M1 and M2 from baseline to completion is shown in Figures 33 to 36, with the exception of the amplitude of the fundamental growing as the test continued.
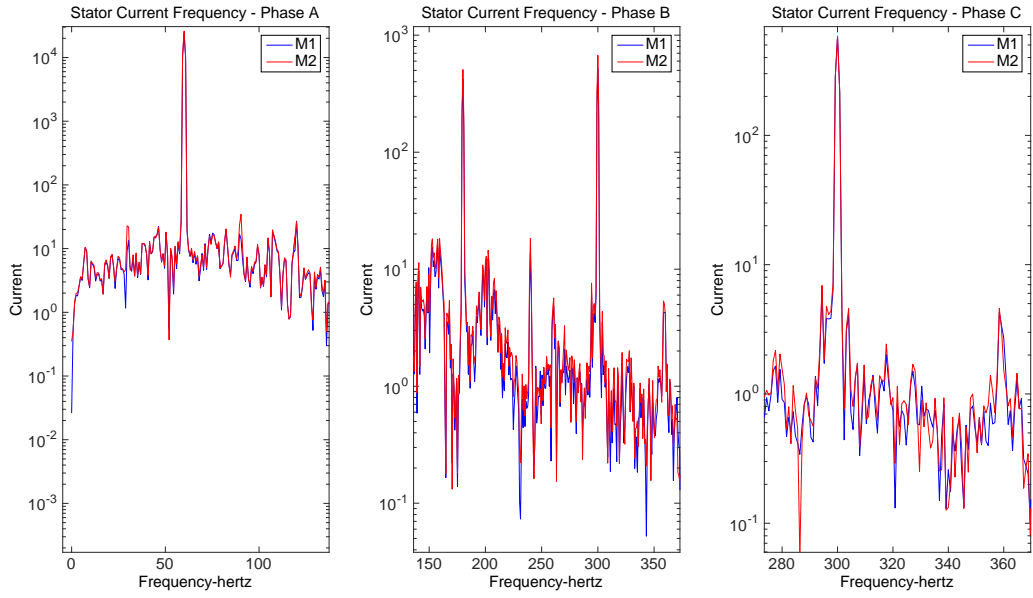
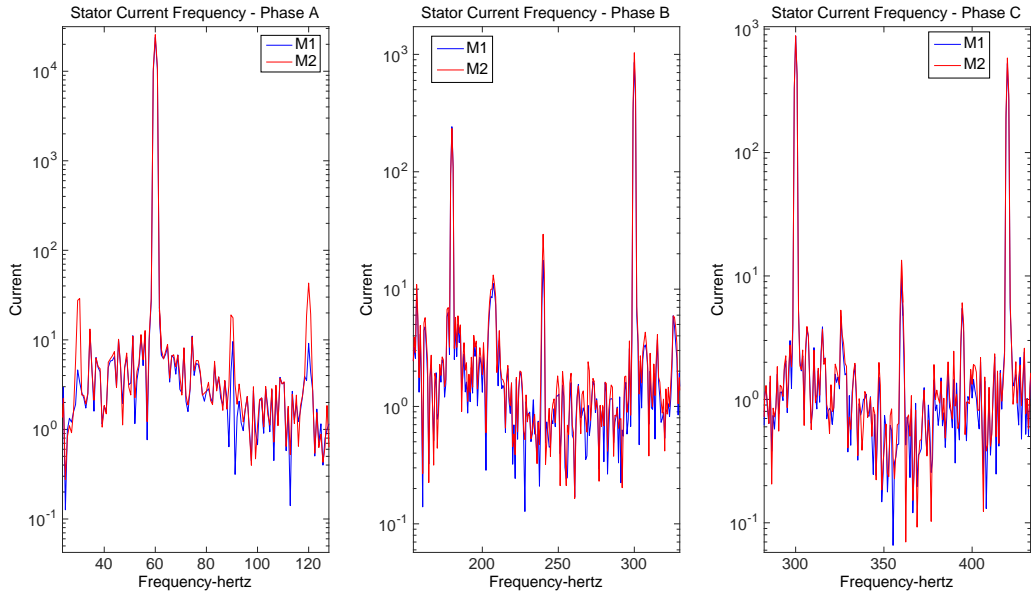Figure 33. Current FFT early in bearing test.
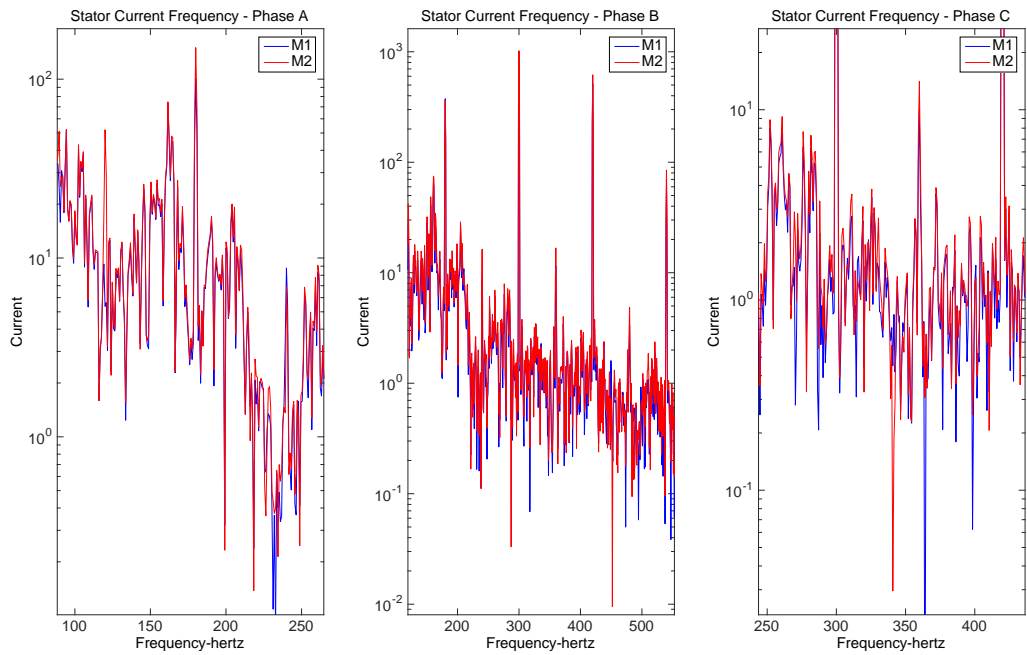

Figure 34. Current FFT middle in bearing test.

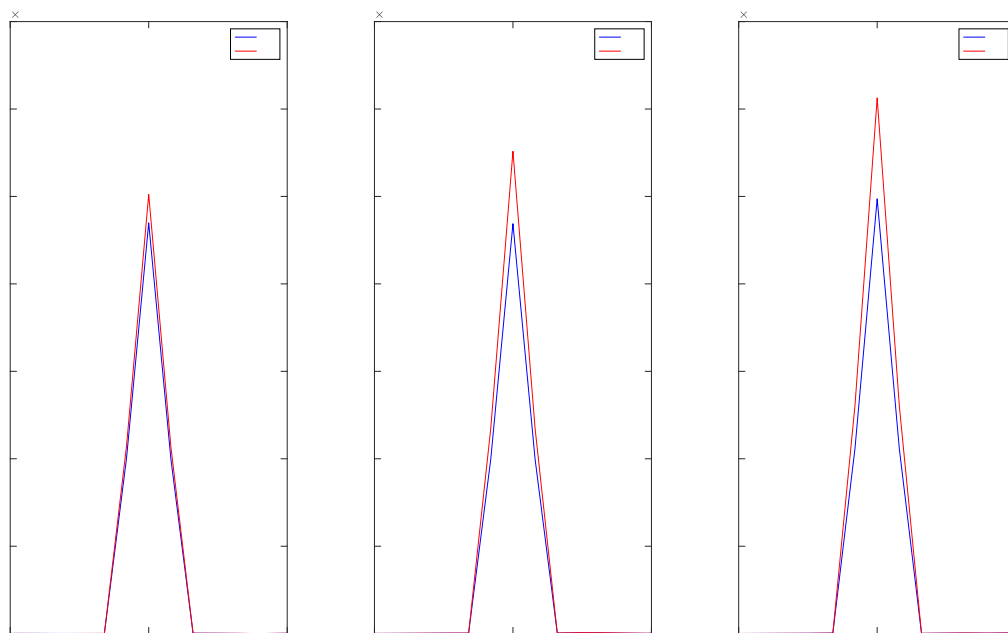Figure 35. Current FFT end in bearing test.

Figure 36. Current FFT end in bearing test in linear scale.

5. SUMMARY AND FUTURE PLANS

This report presents the FY 2015 research activities (completed in FY 2016) associated with the OLM for active components project, and marks the end of the multi-year project. Working with EPRI, INL demonstrated online monitoring for Emergency Diesel Generators and Generator Step-up Transformers in 2013, using EPRI's FW-PHM as a prognostic architecture. In 2014, custom prognostic models for Generator Step-Up Transformers were implemented and demonstrated in FW-PHM.

In 2015, the work focused on developing diagnostic and prognostic models for induction motors, which are commonly used to drive the mechanical pumps used in cooling systems of nuclear reactors. Induction motors are generally known as dependable machines, but are susceptible to faults associated with the electro-mechanical components common to electric spinning machines. Specifically, failures may be more common in the moving parts that support the rotation of the motor due to wear, improper assembly or maintenance, or other damage. Based on this information, the work focused on air-gap eccentricity and bearing-related faults.

The ultimate goal of this research was to demonstrate the use of prognosis for induction motors. With this goal in mind, a series of experiments were performed at ISU's ESTEC to collect relevant data to characterize a damage progression scenario. Two induction motors were instrumented with sensors to periodically record temperature, vibration, and motor current data. One motor was operated in a healthy state to provide baseline data. In order to initiate progressive damage, a loss of bearing lubrication fault was introduced in the second motor. The bearing lubrication was flushed, and the motor was operated for extended period of time with the expectation that the lack of lubrication would degrade the bearing. Temperature, vibration, and motor current data processed, and analyzed to detect any precursor(s) associated with loss of bearing lubrication.

The results of the experiments demonstrated both the resilience of induction motors and the quality of modern lubricants. Little to no evidence of degradation was seen in any of the signals from the non-lubricated motor. It was only the introduction of iron savings at the end of the test that provided clear evidence of damage, but that resulted in an abrupt change in the data signals (appropriate for use in diagnosis) rather than the slow trend desirable for prognosis. Although the results of these experiments were not useful for prognosis, the experimental setup at ESTEC provides a practicable test bed for damage progression scenarios and fault signature validation. It is recommended that any future experiments involve loading the motor, creating higher stress concentrations that would speed up damage instigation.

6. REFERENCES

Agarwal, V., Lybeck, N., Matacia, L., Pham, B., 2013, *Demonstration of Online Monitoring for Generator Step-up Transformers and Emergency Diesel Generators*, INL/EXT-13-30155, September 2013.

Barbieri, F., Hines, W., Sharp, M., and Venturini, M., 2015, "Sensor-Based Degradation Prediction and Prognosis for Remaining Useful Life Estimation: Validation on Experimental Data of Electric Motors," *International Journal of Prognostics and Health Management*, July 2015.

Benbouzid, M. E. H., 2000, "A review of induction motors signature analysis as a medium for faults detecton," *IEEE Transactions on Industrial Electronics, Vol. 47, No. 5, October 2000*.

Benbouzid, M. E. H., M. Vieira, and C. Theys, 1999, "Induction motors' faults detection and localization using stator current advanced signal processing techniques," in *IEEE Transactions on Power Electronics,* Vol.14, No.1, 1999, pp.14–22.

Cameron, J. R., W. T. Thomson, and A. B. Dow, 1986, "Vibration and current monitoring for detecting air gap eccentricity in large induction motors," *IEE Proceedings Electrical Power Applications*, Vol. 133, No. 3, pp. 155–163.

Elkasabgy, N. M., A. R. Eastham, and G. E. Dawson, 1992, "Detection of broken bars in the cage rotor on an induction machine," *IEEE Transactions on Industrial Applications*, Vol. 28, No. 1, pp. 165–171.

EPRI, 2012, *Asset Fault Signature Requirements*, Software manual, Electric Power Research Institute, 2012.

Expert Microsystems, "Fleet-Wide Prognostic Health Management Suite Remaining Life Model Development Guide," unpublished, 2012.

Huang, X., T. G. Habetler, R. G. Harley, and E. J. Wiedenbrug, 2007, "Using a surge tester to detect rotor eccentricity faults in induction motors," *IEEE Transactions on Industrial Applications*, Vol. 43, No. 5, 2007, pp. 1183–1190.

Kral, C., T. G. Habetler, and R. G. Harley, 2004, "Detection of mechanical imbalance of induction machines without spectral analysis of time – domain signals," *IEEE Transactions on Industrial Applications*, Vol. 4, No. 4, pp. 1101–1106.

Kral, C., T. G. Habetler, R. G. Harley, F. Pirker, G. Pascoli, H. Oberguggenberger, and C. J. M. Fenz, 2003, "A comparison of rotor fault detection techniques with respect to the assessment of fault severity," *IEEE international symposium diagnostics for electric machines, power electronics and drives*, pp. 265–270.

Lee, Y. S., J. K. Nelson, H. A. Scarton, D. Teng, D., and S. A. Ghannad, 1994, "An acoustic diagnostic techniques for use with electric machine insulation," *IEEE Transactions on Dielectrics and Electrical Insulation, December 1994,* Vol. 1, No. 6, pp. 1186–1193.

Li, W., and C. K. Mechefske, 2006, "Detection of induction motor faults: A comparison of stator current, vibration and acoustic methods," *Journal Vibration and Control*, Vol. 12, No. 2, February 2006, pp. 165–188.

Lybeck, N.J., J. Coble, M. Tawfik, and L. J. Bond, 2011, "An Assessment of Integrated Health Management (IHM) Frameworks," *3rd International Conference on NPP Life Management (PLiM) for Long Term Operations (LTO)*, May 2012, IAEA-CN-194-031.

Mehrjou, M. R., N. Mariun, M. H. Marhaban, and N. Misron, 2011, "Rotor fault condition monitoring techniques for squirrel-cage induction machine—a review," *Mechanical Systems and Signal Processing*, Vol. 25, No. 8, November 2011, pp. 2827–2848.

Nandi, S., H. A. Toliyat, and X. Li, 2005, "Condition monitoring and fault diagnosis of electrical motors - A review," *IEEE Transactions on Energy Conversion*, Vol. 20, No. 4, pp. 719–729.

Onel I. Y., and M. H. Benbouzid, 2008, "Induction Motor Bearing Failure Detection and Diagnosis: Park and Concordia Transform Approaches Comparative Study," *IEEE/ASME Transactions on Mechatronics*, Vol. 13, No. 2, pp. 257–262.

Penrose, H. W., and J. Jette, 2000, "Static motor circuit analysis: An introduction to theory and application," *IEEE Electrical Insulation Magazine*, Vol. 16, No. 4, July–August 2000, pp. 6–10.

Siau, J., A. Graff, W. Soong, and N. Ertugrul, 2004, "Broken bar detection in induction motors using current and flux spectral analysis," *Australian Journal of Electrical and Electronics Engineering*, Vol. 1, No. 3, 2004, pp. 171–177.

Siddique, A., G. S. Yadava, and B. Singh, B., 2005, "A review of stator fault monitoring techniques of induction motors," *IEEE Transactions on Energy Conversion*, Vol. 20, No. 1, March 2005, pp. 106–114.

Supangat, R., J. Grieger, N. Ertugrul, W. L. Soong, D. A. Gray, and C. Hansen, 2007, "Detection of broken rotor bar faults and effects of loading in induction motors during rundown," *In Proceedings of the IEEE international electric machines and drives conference*, 2007, pp. 196–201.

Tanaka, T., 1995, "Partial discharge pulse distribution pattern analysis," *Proceedings of IEEE Science and Measurements Technologies, January 1995*, Vol. 142, pp. 46–50.

Tavner, P. J., B. G. Gaydon, and D. M. Ward, 1986, "Monitoring generators and large motors," *Proceedings of Institute of Electrical Engineering B, 1986,* Vol. 133, No. 3, pp. 169–180.

Tetrault, S. M., G. C. Stone, and H. G. Sedding, 1999, "Monitoring partial discharges on 4-kV motor windings," *IEEE Transactions on Industrial Applications*, Vol. 35, No. 3, June 1999, pp. 682–688.

Thorsen, O. V., and M. Dalva, 1997, "Condition monitoring methods, failure identification and analysis for high voltage motors in petrochemical industry," *Eighth International Conference on Electrical Machines and Drives, September 1–3, 1997,* pp. 109–113.

Appendix A

Component Name; Induction Motor

Appendix A

Component Name; Induction Motor

Fault Signatures	Fault Features			
	Exam Location	**Technical Exam**	**Value**	**Effectiveness**
Air Gap Eccentricity	Air gap	Drive current	Amplitude	High
	Air gap	Vibration sensor	Amplitude	Medium
	Air gap	Tachometer	Speed reduction without change in load	Low
	Air gap	Thermo couples	Temperature	Low
Broken Rotor Bar(s)	Rotor bar	Drive current	Amplitude	High
	Rotor bar	Vibration sensor	Amplitude	Medium
	Rotor bar	Tachometer	Speed reduction without change in load	Low
Bearing Damage	Bearing	Drive current	Amplitude	High
	Bearing	Vibration	Amplitude	High
	Bearing	Thermocouple	Temperature increase	Medium
Bearing Lubricant Degradation	Bearing	Vibration	Amplitude	Medium